UNC-5081
UC-25, Metals, Ceramics, and Materials
SPECIAL

CARBIDE FUEL DEVELOPMENT

Phase V Report

Period of
October 1, 1962 to September 30, 1963

Authors

United Nuclear

A. Strasser
D. Stahl

The Carborundum Company

K. Taylor
J. Andersen

June 30, 1964

Work Performed under UNC Project 2192
Contract AT(30-1)-2899
with the United States Atomic Energy Commission

Prime Contractor
UNITED NUCLEAR CORPORATION
Development Division
White Plains, New York

Subcontractor
THE CARBORUNDUM COMPANY
Niagara Falls, New York

DISCLAIMER

This report was prepared as an account of work sponsored by an agency of the United States Government. Neither the United States Government nor any agency Thereof, nor any of their employees, makes any warranty, express or implied, or assumes any legal liability or responsibility for the accuracy, completeness, or usefulness of any information, apparatus, product, or process disclosed, or represents that its use would not infringe privately owned rights. Reference herein to any specific commercial product, process, or service by trade name, trademark, manufacturer, or otherwise does not necessarily constitute or imply its endorsement, recommendation, or favoring by the United States Government or any agency thereof. The views and opinions of authors expressed herein do not necessarily state or reflect those of the United States Government or any agency thereof.

DISCLAIMER

Portions of this document may be illegible in electronic image products. Images are produced from the best available original document.

FOREWORD

The Carbide Fuel Development project is sponsored by the USAEC Division of Reactor Development. United Nuclear Corporation is performing the conceptual design, fuel evaluation, and fuel irradiation. Under its prime contract with the AEC, the United Nuclear Corporation, Development Division, has issued a subcontract to The Carborundum Company for fuel fabrication. Both companies are operating plutonium handling facilities.

The report summarizes progress from October 1, 1962 through September 30, 1963.

Previous progress was reported in:

NDA 2140-2, Carbide Fuel Development – Phase I Report (Oct. 15, 1959)
NDA 2145-1, Carbide Fuel Development – Progress Report (Mar. 11, 1960)
NDA 2145-4, Carbide Fuel Development – Progress Report (June 13, 1960)
NDA 2145-5, Carbide Fuel Development – Progress Report (Aug. 30, 1960)
NDA 2145-6, Carbide Fuel Development – Phase II Report (Nov. 6, 1960)
NDA 2162-1, Carbide Fuel Development – Progress Report (Feb. 28, 1961)
NDA 2162-3, Carbide Fuel Development – Progress Report (June 1, 1961)
NDA 2162-5, Carbide Fuel Development – Phase III Report (Sept. 30, 1961)
UNC-5003, Carbide Fuel Development – Progress Report (Feb. 9, 1962)
UNC-5013, Carbide Fuel Development – Progress Report (May 28, 1962)
UNC-5030, Carbide Fuel Development – Progress Report (Aug. 10, 1962)
UNC-5055, Carbide Fuel Development – Phase IV Report (Mar. 31, 1963)
UNC-5056, Carbide Fuel Development – Progress Report (May 1, 1963)
UNC-5068, Carbide Fuel Development – Progress Report (Sept. 30, 1963)

CONTENTS

1. INTRODUCTION 1

2. SUMMARY AND CONCLUSIONS 3
   2.1 Fuel Fabrication and Evaluation 3
   2.2 Irradiation Tests 4

3. FUEL FABRICATION AND EVALUATION 5
   3.1 Powder Preparation 5
      3.1.1 Synthesis of $(U_{0.95}Pu_{0.05})C_{0.98}$ 5
      3.1.2 Synthesis of $(U_{0.8}Pu_{0.2})_2C_3$ 7
      3.1.3 Synthesis of Carbon-Stabilized PuO 8
      3.1.4 Synthesis of Carbon Stabilized $(U_{0.8}Pu_{0.2})O$ 9
   3.2 Sample Fabrication 11
      3.2.1 Fabrication of $(U_{0.95}Pu_{0.05})C_{0.98}$ Samples for Property Measurements 11
      3.2.2 Fabrication of $(U_{0.8}Pu_{0.2})_2C_3$ Pellets 17
   3.3 Vacuum Annealing Experiments 17
   3.4 Effect of Aging on Lattice Parameters 25
   3.5 Microprobe Analyses 25
   3.6 Fuel Clad Compatibility 27
   3.7 Coefficient of Thermal Expansion Measurements 32
   3.8 Melting Point Determinations 42
   3.9 Vapor Pressure Measurements 42
      3.9.1 Introduction 42
      3.9.2 Experimental Equipment 44
      3.9.3 Knudsen Cell Design 44
      3.9.4 System Geometry Calibration 46

4. IRRADIATION TESTS 47
   4.1 Experiment Design and Assembly 47
   4.2 Experiment Operation 49
   4.3 In-Pile Thermal Conductivity 58

4.4 Post-Irradiation Examination of Capsules 61 and 64 60
4.4.1 Summary 60
4.4.2 Visual Examination and Gamma Scanning 63
4.4.3 Fission Gas Release 63
4.4.4 Macro Examination 66
4.4.5 Micro Examination 69
4.4.6 Plutonium Distribution 80
4.4.7 Burnup Determination 81
4.4.8 Hot Cell Handling Procedure 81

TABLES

1. Analyses of Raw Materials for Fuel Synthesis 6
2. Synthesis of $(U_{0.95}Pu_{0.05})C_{0.98}$ Solid Solution 7
3. Synthesis of Carbon-Stabilized Plutonium Monoxide 8
4. Results of Experiments to Synthesize $(U_{0.8}Pu_{0.2})O$ 12
5. Results of Sintering Experiments With $(U_{0.95}Pu_{0.05})C_{0.98}$ Pellets . 15
6. Results of Sintering Experiments With $(U_{0.95}Pu_{0.05})C_{0.98}$ Bars . . 18
7. Results of Sintering Experiments With $(U_{0.8}Pu_{0.2})_2C_3$ 19
8. Effect of Vacuum Annealing on $(U_{0.8}Pu_{0.2})C_{0.95}$ Pellets Previously Sintered in Helium 22
9. Effect of Aging on Lattice Parameter of $(U_{0.95}Pu_{0.05})C_{0.98}$ Powder (Camera Method) 26
10. Effect of Aging on the Lattice Parameter of $(U_{0.8}Pu_{0.2})C_{0.95}$ Powder (Diffractometer Method) 26
11. Fuel-Type 316 Stainless Steel Compatibility 29
12. Fuel-2¼ Cr-1 Mo Steel Compatibility 32
13. Fuel-Niobium, Niobium-1% Zirconium Compatibility 33
14. Summary of Carbide Thermal Expansion Coefficients 38
15. Coefficient of Expansion of $(U_{0.95}Pu_{0.05})C_{0.98}$ 39
16. Coefficient of Expansion of $(U_{0.95}Pu_{0.05})C_{0.98}$ + 0.1 w/o Ni 39
17. Coefficient of Expansion of Arc-Cast UC 40
18. Analysis of Thermal Expansion Bars 40
19. Silver Vapor Pressure Test 46
20. Summary of Average Operating Conditions of Specimens 62, 63, 65, and 66 During GETR Cycle 47 (September 1963) 52
21. Summary of Irradiation Conditions for Specimens 61T, 61B, 64T, and 64B 57
22. Helium Gap Conductances (w/cm^2-°C) for UC Irradiation Specimens 61
23. Summary of Post-Irradiation Examination Results 64
24. Dimensional and Density Measurements of Whole Pellets 68

25. Microhardness of Irradiated Type 316 Cladding 75
26. Radial Variation of Burnup in Fuel 82

FIGURES

1. Carbon stabilized PuO 10
2. Reaction Product from $(U_{0.8}Pu_{0.2})O$ Synthesis 13
3. Typical Structure of $(U_{0.95}Pu_{0.05})C_{0.98}$ 16
4. Typical Structure of $(U_{0.95}Pu_{0.05})C_{0.98}$ + 0.1 w/o Ni 16
5. Solid Solution Sesquicarbide $(U_{0.8}Pu_{0.2})_2C_3$ 20
6. $(U_{0.8}Pu_{0.2})C_{0.95}$ + 0.1 w/o Ni – as Sintered in Helium at 1550°C, 1/2 hr 23
7. $(U_{0.8}Pu_{0.2})C_{0.95}$ + 0.1 w/o Ni – sintered in Helium and Vacuum Annealed at 1900°C, 1 hr 23
8. $(U_{0.8}Pu_{0.2})C_{0.95}$ + 0.1 w/o Ni – Sintered in Helium and Vacuum Annealed at 2200°C, 1/2 hr 23
9. $(U_{0.8}Pu_{0.2})C_{0.95}$ – as Sintered in Helium at 1925°C, 1 hr 24
10. $(U_{0.8}Pu_{0.2})C_{0.95}$ – Sintered in Helium and Vacuum Annealed at 2200°C, 1/2 hr 24
11. Compatibility Capsule 28
12. Type 316 Stainless Steel from Compatibility Test 30
13. 2¼ Cr-1 Mo Steel from Compatibility Test 31
14. Niobium from Compatibility Test 34
15. Niobium-1% Zirconium from Compatibility Test 35
16. Zircaloy-2 from Compatibility Test 36
17. Schematic of Dilatometer 41
18. Temperature Correction Curve Based on Melting of Standards . . 43
19. Schematic of Thermal Stability Experiment 45
20. Irradiation Specimens – Cross Sectional View 48
21. Irradiation Capsule – Cross Sectional View 50
22. Thermocouple Records – 61T and 61B 53
23. Thermocouple Records – 64T and 64B 54
24. Specimen Temperature Histories – 61T and 61B 55
25. Specimen Temperature Histories – 64T and 64B 56
26. Schematic of In-Pile Thermal Conductivity Measurement 59
27. Typical In-Pile Measurements of Conductivities and Conductances 62
28. Clad $(U_{0.8}Pu_{0.2})C_{0.95}$ Fuel Specimens After Irradiation 65
29. Typical Irradiated Fuel Pellets 67
30. ID of Clad Bend Tests 70

31. $(U_{0.8}Pu_{0.2})C_{0.95}$ + 0.1 w/o Ni Microstructure 71
32. $(U_{0.8}Pu_{0.2})C_{0.95}$ Microstructure 72
33. Typical Type 316 Stainless Steel Clad Microstructure after 2190 hr 73
34. Magnification of Failed Section – Specimen 64B 76
35. Representative Microstructures from the Failed Section 77
36. Reaction Zones in Ruptured Type 316 Cladding 79
37. Cross Section of Fuel Pellet after Removing Samples for Plutonium Distribution Analysis 80

1. INTRODUCTION

The Carbide Fuel Development Program is concerned with the technology of the entire UC-PuC fuel cycle. The major goal of the program is to produce (UPu)C and obtain data on its irradiation behavior for long burnups and at high power generation rates. In addition, other areas of the fuel cycle are being explored to discover possible problems.

Fuel made of a combination of UC and PuC has a potential of reducing the fuel cycle cost of existing fast breeder reactors. This is because of the increased burnup and increased power generation capability of (UPu)C compared to presently available metallic fuels. However, irradiation tests to 8×10^{20} fiss/cm^3 show that (UPu)C is dimensionally more stable than metallic fuel, and that it releases less fission gas than oxide fuel irradiated at comparable power. Because of the high melting point and good thermal conductivity of UC and (UPu)C, there is further expectation that carbide fuels will be capable of high power generation rates. The program was initiated in May 1959 and as originally outlined covers a period of about $4\frac{1}{2}$ yr. Program objectives are outlined below.

Conceptual Design

1. An analytical study of the effect of substitution of (UPu)C on heat transfer, physics, and cost of existing fast breeder reactors.
2. Conceptual design of rod-type, fuel element configurations which can be substituted directly in existing reactors.

The above was completed and reported in NDA 2140-2.

Facility Design and Fabrication

1. Design and construction of a facility for carbide fabrication at The Carborundum Company.
2. Design and construction of a facility for carbide evaluation at United Nuclear.

The above was completed and reported in NDA 2145-6.

Fuel Fabrication and Evaluation

1. Explore various methods for preparation of fuel from powders and fabrication of the fuel into cylindrical pellets. High density (up to 13.2 g/cm^3) UC and (UPu)C pellets have been made. The preparation of sesquicarbides and carbon stabilized monoxides was studied.
2. Evaluate pellets by density measurement, chemical analysis, X-ray diffraction, metallography; perform fuel-cladding compatibility studies; measure physical constants. This is complete for UC and in process for (UPu)C. The (UPu)C melting point is being measured and the coefficient of expansion measurements are complete. The majority of the compatibility tests is complete.

Fuel Irradiation

1. Irradiate clad fuel samples with burnup and maximum fuel temperature as the major variables.
2. A minimum 2% burnup of all fuel atoms by fission and a mimimum 650°C (1200°F) central fuel temperature were selected to establish the economic advantages of the fuel.

The UC samples have been irradiated and examined (NDA 2162-5, UNC-5055). Eight (UPu)C samples are being irradiated, and the irradiation of four samples has been completed. Their post-irradiation examination is in progress.

2. SUMMARY AND CONCLUSIONS

2.1 FUEL FABRICATION AND EVALUATION

Test samples of solid solution $(U_{0.95}Pu_{0.05})C_{0.98}$ for physical property measurement were fabricated by cold pressing and sintering powders prepared by the carbon reduction of oxides. The preparation of $(U_{0.8}Pu_{0.2})_2C_3$ was studied by a similar method.

The preparation of PuO and $(U_{0.8}Pu_{0.2})O$ was studied. Products containing predominantly monoxide were identified.

Vacuum annealing studies of $(U_{0.8}Pu_{0.2})C_{0.95}$ and $(U_{0.8}Pu_{0.2})C_{0.95}$ + 0.1 w/o Ni showed that the oxygen and nickel contents could be reduced significantly.

The effect of aging on the lattice parameter of $(U_{0.95}Pu_{0.05})C_{0.98}$ and $(U_{0.8}Pu_{0.2})C_{0.95}$ was found to be insignificant in periods up to 7 months.

Microprobe analyses of $(U_{0.8}Pu_{0.2})C_{0.95}$ + 0.1 w/o Ni showed good plutonium and nickel uniformity.

Compatibility tests between $(U_{0.95}Pu_{0.05})C_{0.98}$ with and without nickel vs type 316 stainless steel, 2¼ Cr-1 Mo steel, niobium, niobium-1 w/o zirconium, and Zircaloy-2 up to 4000 hr and 816°C showed no reactions except for Zircaloy-2 and one sample of niobium-1 w/o zirconium.

The coefficient of expansion of $(U_{0.95}Pu_{0.05})C_{0.98}$ at 25 to 1400°C was measured as 12.6×10^{-6}/°C, and that of $(U_{0.95}Pu_{0.05})C_{0.98}$ + 0.1 w/o Ni at 25 to 1400°C was measured as 12.2×10^{-6}/°C.

An initial melting point measurement of $(U_{0.95}Pu_{0.05})C_{0.98}$ gave 2500°C.

2.2 IRRADIATION TESTS

Twelve samples of clad $(U_{0.8}Pu_{0.2})C_{0.95}$ were inserted in the test reactor, and the irradiation of four of the samples was completed at their target burnups of 5.0 to 6.8×10^{20} fiss/cm^3 (15,700 to 21,400 MW-d/T) average.

The post-irradiation examination in progress for the four specimens irradiated 355 to 395 w/cm average at fuel center temperatures of 1000 to 1400°C and clad surface temperatures of 600 to 800°C shows that with the exception of a localized rupture the stability of the fuel is excellent. The clad dimensions did not change, fission gas release was low (the amount expected from recoil), fuel dimensional changes were relatively small (up to 5% volume increase), and the microstructure of the fuel did not change. The cause for a localized rupture in one specimen is believed to be an operating defect of the irradiation capsule.

The in-pile thermal conductivity of the fuel in the temperature range of 700 to 1000°C was estimated to be an average of 0.046 cal/sec-cm^2-°C/cm. This compares favorably with out-of-pile measurements, and is about 84% of the value for UC.

3. FUEL FABRICATION AND EVALUATION

3.1 POWDER PREPARATION

3.1.1 Synthesis of $(U_{0.95}Pu_{0.05})C_{0.98}$

The current program is evaluating the out-of-pile properties of mixed uranium-plutonium carbides at the 5 w/o Pu level. A total of about 400 g of $(U_{0.95}Pu_{0.05})C_{0.98}$ powder was synthesized for the fabrication of test specimens.

Fifty-gram reaction mixes of PuO_2, UO_2, and carbon were blended, cold-pressed without binder at about 5000 psi (pellets about 0.2 in. in diameter), and heated in helium to 1625°C with a hold time of $5\frac{1}{2}$ hr. Results of the analyses of the starting materials are given in Table 1. The reaction end-point was determined by monitoring the exhaust gas, drawn from the heated furnace, for CO. The results of analyses for total carbon and X-ray diffraction, as determined on the pulverized reaction products, are shown in Table 2.

The carbide powders, resulting from the eight synthesis experiments, were combined and subsequently ball-milled for 24 hr in a rubber-lined mill using stainless steel balls. X-ray diffraction of the composite showed single-phase (UPu)C with a unit cell size, $a_0 = 4.959 \pm 0.001$ Å. The results of analyses for total carbon gave 4.79 w/o. The intended carbon content was 4.70 w/o.

Table 1 — Analyses of Raw Materials for Fuel Synthesis (parts per million)

Element	PuO_2*	UO_2†	C‡	Ni§
Ag	< 10	< 0.01		n.d.¶
Al	< 50	5	0	10-50
As	<100			
B	< 0.5	0.1		n.d.
Ba	< 1			
Be	< 0.1			
Bi	< 10			
Ca	20	< 5	<10	10-50
Cd	< 10	< 0.2		
Co		< 1		100-500
Cr	< 30	5		1-5
Cu	< 20	0.1	< 2	10-50
F		60		
Fe	<100	40	< 3	100-500
Ga	< 10			n.d.
K	< 1			
La	< 50			
Mg	< 10	2	2	
Mn	< 5	2	< 1	10-50
Mo	< 10	0.5		1-5
Na				2
Ni	< 30	10		
P	< 50			
Pb	< 10	1		
Pd	< 20			
Sb	< 10			
Si	< 10	40	30	100-500
Sn	< 10	< 1		
Sr	< 20			
Ta	<200			
Te	< 20			
Ti	< 10	1	< 2	5-10
Tl	< 20			
V	< 10	< 1	< 2	n.d.
W		< 5		n.d.
Zn	20			
Zr	<100		9	1-5
Total detectable impurities	40	~170	60	

*Made by the ignition of metal, by Dow Chemical Company.
†Ceramic grade, made by Mallinckrodt Corp.
‡Made by cracking of methane, by Cabot Co.
§Minus 325 mesh powder, hydrogen reduced.
¶Not detected.

Table 2 — Synthesis of $(U_{0.95}Pu_{0.05})C_{0.98}$ Solid Solution
(1625°C – 5½ hr Hold Time – Normal U)

Experiment No.	Total Carbon, w/o	Results of X-Ray Analysis
1	4.94	Single-phase (UPu)C, $a_0 = 4.9610 \pm 0.0003$ Å
2	4.88	
3	4.74	
4	4.66	Single-phase (UPu)C, $a_0 = 4.9618 \pm 0.0003$ Å
5	4.78	
6	4.76	
7	4.73	
8	4.79	

3.1.2 Synthesis of $(U_{0.8}Pu_{0.2})_2C_3$

The sesquicarbides may have potential advantages over the monocarbides. Preliminary experiments were started to obtain some information on the fabrication technology and properties of the compound.

Two experiments were performed to synthesize $(U_{0.8}Pu_{0.2})_2C_3$. Stoichiometric proportions of PuO_2, UO_2, and carbon were blended and cold compacted, without binder, at 30,000 psi. Results of the analyses of the starting materials are given in Table 2. These reaction pellets were about 0.2 in. in diameter and weighed about 1 g each. The reaction pellets were heated to 1650°C with a hold time of 4 hr. Four grams of material were reacted in the first experiment and 25 g in the second. Chemical analyses on the pulverized products gave total carbon at 6.98 w/o and 6.95 w/o, respectively, for the two experiments. The theoretical carbon content is 7.02 w/o. The results of X-ray analyses, taken on a representagive sample from the 4-g synthesis, showed a major $(UPu)_2C_3$ phase, a faint UC type structure, and a faint phase which could not be identified. The unit cell size for the sesquicarbide phase was $a_0 = 8.108 \pm 0.002$ Å. The ASTM index card gives $a_0 = 8.129$ for Pu_2C_3 and $a_0 = 8.088$ for U_2C_3.

3.1.3 Synthesis of Carbon-Stabilized PuO

The monoxides should have better corrosion resistance and a thermal conductivity equivalent to that of the monocarbides (therefore, better than the dioxides). Attempts by other investigators to make massive UO have been unsuccessful, but the ability of carbon to stabilize UO has been established. The preparation of massive PuO, on the other hand, has been reported by Harwell and Hanford.

The goals of this study were to identify PuO and $(U_{0.8}Pu_{0.2})O$ as possible products of the oxide-carbon reaction and to determine whether these compounds could be made in massive form. The apparent stability of PuO and the ability of small amounts of carbon to stabilize monoxides offers hope of a stable mixed monoxide.

Initial experiments to synthesize PuO utilized the carbon reduction of PuO_2. Carbon and PuO_2 were combined in stoichiometric proportions to form PuO, then blended and pressed without a binder into 0.2-in. diameter pellets at 30,000 psi. Results of the analyses of the starting materials are given in Table 1. The pellets were reacted in the helium atmosphere furnace at 1750°C for 5½ to 6 hr. The exhaust gas, drawn from the heated furnace, was monitored periodically for CO to determine the reaction end-point. The reacted products were crushed in the Spex mixer and chemical analyses were made. Results are shown in Table 3.

Table 3 — Synthesis of Carbon-Stabilized Plutonium Monoxide

Experiment No.	Synthesis Temp, °C	Time, hr	Total Carbon, w/o	Results of X-Ray Analysis	Comment
1	1750	5½	0.17	Several UC type phases (PuC, PuO, PuN)	Cored
2	1750	6	0.15	Single-phase UC type structure	Cored

Lattice parameters could not be determined because of weak film intensity and the poor resolution.

As shown in Fig. 1, metallographic examination of the synthesized clinker showed a two-phase structure, a major gray phase (probably PuO with some carbon impurity), and a white phase (probably α Pu_2O_3). The structure was unaffected by the normal carbide etch (nitric-acetic acids), and was slightly affected by the normal oxide etch (nitric-hydrofluoric).

An initial experiment at 1800°C on a tantalum setter resulted in a fused pellet stuck to the tantalum. The reason for the fusion is not known. It may have been either an indication of the PuO melting point, or the result of the PuO_2-Ta reaction. Tantalum and tungsten setters were compared in the 1750°C experiments described in Table 3. Both metals were satisfactory at 1750°C; however, less sticking was encountered with tungsten.

3.1.4 Synthesis of Carbon Stabilized $(U_{0.8}Pu_{0.2})O$

Several experiments were performed in an attempt to synthesize $(U_{0.8}Pu_{0.2})O$. The existence and stability of the pure, mixed monoxide phase are unknown. However, the existence of a carbon stabilized (UPu)O is very likely. The identification of (UPu)(OC) type compounds is important, since there are significant quantities of oxygen present in the (UPu)C produced by the oxide-carbon reaction. In addition, such a compound could have desirable engineering properties: the oxidation resistance of an oxide and the thermal conductivity of a monocarbide.

For reaction purposes, PuO_2 and C in stoichiometric proportions to give $(U_{0.8}Pu_{0.2})O$ were intimately blended and pressed, without binder, into 0.2-in. diameter pellets. Results of the analyses of the starting materials is given in Table 1. The forming pressure was 30,000 psi.

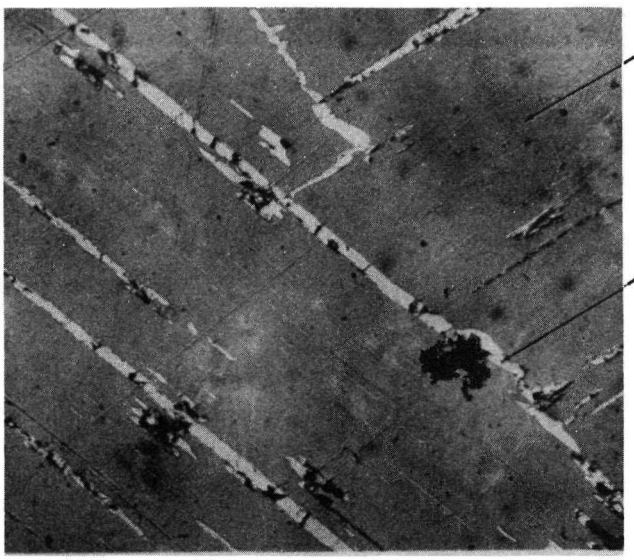

Fig. 1 — Carbon stabilized PuO. Made by synthesis of PuO_2 plus C at 1750°C, 6 hr. 600×. Unetched.

For synthesis, the temperatures investigated were 1650, 1750, 1850, 1950, and 2000°C. The results of this study are shown in Table 4.

Metallographic examination of the product from Experiment 8 showed a two-phase structure, a gray dioxide-type phase, and a light monoxide-type phase, each about 50% in volume. (See Fig. 2.)

The method of synthesis produces a product of about 1 w/o carbon containing a mixture of dioxide- and monoxide-type phases. The carbon distribution between the two phases is unknown at this time.

3.2 SAMPLE FABRICATION

3.2.1 Fabrication of $(U_{0.95}Pu_{0.05})C_{0.98}$ Samples for Property Measurements

The $(U_{0.95}Pu_{0.05})C_{0.98}$ powder described in Table 2 was used to fabricate pellets for melting point, vapor pressure, and compatibility specimens, and to fabricate bars for thermal coefficient of expansion measurements.

Seventy pellets were fabricated, of which 35 contained 0.1 w/o nickel.

Compacts containing nickel were prepared by blending with nickel powder in the ball mill for at least 2 hr. The analysis of the nickel is given in Table 1. The nickel was prepared by the hydrogen reduction of minus 325 mesh powder at 700°C, followed by ball milling in the rubber lined mill with the stainless steel balls.

The powder with and without nickel was mixed with 1/4 w/o Carbowax 6000 binder and cold pressed at 30,000 psi. The size of the cold-pressed pellets was 0.224 in. in diameter by 0.215 in. high. The pellets were preheated to about 700°C in an open tantalum crucible to volatilize the binder. The final sintering was completed in a closed tantalum crucible. Pellets without the nickel sintering aid were heated to 1925°C with a hold time of 1 hr; those containing the 0.12 w/o addition of nickel

Table 4 — Results of Experiments to Synthesize $(U_{0.8}Pu_{0.2})O$

Experiment No.	Reaction Temp, °C and Hold Time	Batch Size, g	Total Carbon, w/o	X-Ray Analysis (Diffractometer)
1	1650 – 5 hr	5	1.09	Major 2-phase $(UPu)O_2$ type $a_0 = 5.482 \pm 0.002$ Å $a_0 = 5.4732 \pm 0.0009$ Å Moderate/Strong (UPu)O or (UPu)C type $a_0 = 4.9565 \pm 0.0002$ Å Indication of UC_2
2	1750 – 6 hr	5	0.96	Major, 3 distinct $(UPu)O_2$ type phases $a_0 = 5.4938 \pm 0.0007$ Å $a_0 = 5.4841 \pm 0.0009$ Å $a_0 = 5.475 \pm 0.001$ Å Moderate (UPu)O or (UPu)C type $a_0 = 4.9540 \pm 0.0007$ Å
3	1850 – 3½ hr	5	0.98	Major, 2 distinct $(UPu)O_2$ type phases $a_0 = 5.4959 \pm 0.0009$ Å $a_0 = 5.4864 \pm 0.0003$ Å Weak (UPu)O or (UPu)C type $a_0 = 4.945 \pm 0.003$ Å
4	Product from Exp. 3 crushed, pressed, and reheated to 2000 – 2 hr		0.65	Major, several $(UPu)O_2$ type phases Avg. $a_0 = 5.473$ Å Moderate (UPu)O or (UPu)C type $a_0 = 4.9453 \pm 0.0008$ Å Indication of UC_2
5	1850 – 3 hr	30	1.11	Not determined
6	Product from Exp. 5 crushed, pressed, and reheated to 1850 – 1 hr		1.00	Not determined
7	Product from Exp. 6 crushed, pressed, and reheated to 1850 – 2 hr		1.07	Major $(UPu)O_2$ type $a_0 = 5.4908 \pm 0.0005$ Å Moderate (UPu)O or (UPu)C type $a_0 = 4.9456 \pm 0.0006$ Å
8	Product from Exp. 7 crushed, pressed, and reheated to 2000 – 1 hr		0.90	Major, several $(UPu)O_2$ type phases Avg. $a_0 = 5.4929 \pm 0.0006$ Å Moderate/Strong, several (UPu)O or (UPu)C type phases* Avg. $a_0 = 4.9429 \pm 0.0007$ Å
9	1950 – 3 hr	5	0.75	Not determined
10	Pellets from Exp. 9 reheated to 2000 – 2 hr		0.82	Not determined
11	2000	5	0.98	Major, several $(UPu)O_2$ type phases Avg. $a_0 = 5.486$ to 5.494 Å Moderate/Strong, several (UPu)O or (UPu)C type phases Avg. $a_0 = 4.943$ to 4.956 Å

*Metallography and etchants identified the face-centered cubic phase as monoxide rather than monocarbide.

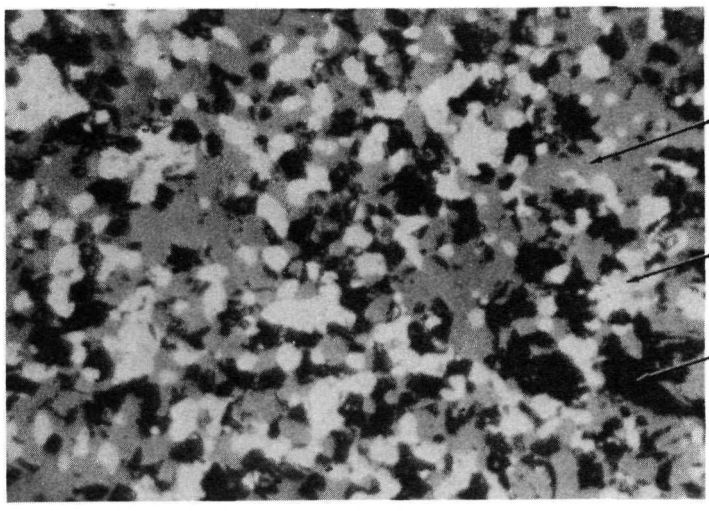

Fig. 2 — Reaction product from $(U_{0.8}Pu_{0.2})O$ synthesis. 600×. Unetched. (Experiment 8, Table 4)

were sintered at 1550°C with a hold time of 1/2 hr. Results of these experiments are shown in Table 5.

Metallographic examination of $(U_{0.95}Pu_{0.05})C_{0.98}$ (Figs. 3, 4) showed structures similar to those of $(U_{0.8}Pu_{0.2})C_{0.95}$. Material without sintering aid was essentially single-phase monocarbide with some Widmanstätten structure. Material with nickel sintering aid contained sesquicarbide in the monocarbide matrix.

Eight $(U_{0.95}Pu_{0.05})C_{0.95}$ coefficient of expansion bars, 2.230 in. long, 0.233 in. wide, and 0.340 in. high, were fabricated, four with nickel sintering aid and four without.

Problems involving warpage and breakage of the bars during the sintering operation were anticipated. To conserve the limited supply of $(U_{0.95}Pu_{0.05})C_{0.98}$ powder, several exploratory sintering experiments were conducted with UC. The results of these experiments indicated that the specimens were too fragile to handle after the usual presintering step at 700°C. This step is normally carried out in an open tantalum crucible to volatilize the binder, and the final sinter is then completed in a closed tantalum crucible. To minimize warpage in the bars without the nickel addition, it was necessary to presinter at 1550°C to provide sufficient strength for handling, and to confine the bars closely in a tantalum-lined graphite crucible before the final sintering at 1925°C.

The bars were cold pressed at 13,000 psi (maximum pressure attainable with the existing pressing equipment) and contained the usual 1/4 w/o Carbowax binder. The bars, with and without the nickel additions, subsequently were sintered for 1 hr at 1550 and 1925°C, respectively. The bars containing the nickel addition met size and camber specifications after the sintering operation, and grinding was unnecessary. However, those without the nickel addition were warped excessively.

Two of these bars were reheated to 1850°C with a hold time of 1/4 hr in an attempt to decrease the camber along the longitudinal and lateral axes. These bars were

Table 5 — Results of Sintering Experiments With $(U_{0.95}Pu_{0.05})C_{0.98}$ Pellets

[Pellet Density, g/cm^3 (10 Pellets)]

Experiment No.	Sintering Conditions	Intended Composition	Range	Average	Plutonium,* %	Total Carbon,† w/o	Nitrogen, ppm	X-Ray Analysis
1	1925°C, 1 hr	$(U_{0.95}Pu_{0.05})C_{0.98}$	12.24-13.37	12.31	4.9	4.67	273	Single-phase (UPu)C $a_0 = 4.9616 \pm 0.0003$ Å
2	1550°C, 1/2 hr	$(U_{0.95}Pu_{0.05})C_{0.98}$ plus 0.1 w/o Ni	12.93-13.15	13.04	4.6	4.79	144	Single-phase (UPu)C $a_0 = 4.961 \pm 0.001$ Å

*Intended plutonium content: 4.75%.
†Intended carbon content: 4.70 w/o.

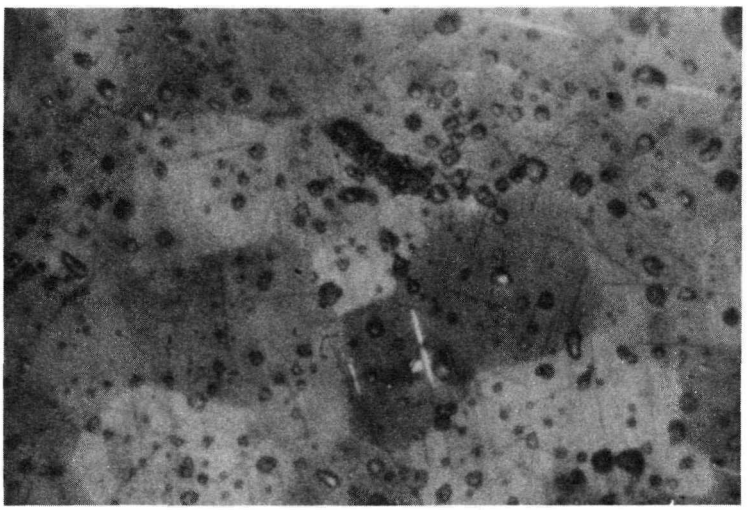

Fig. 3 — Typical structure of $(U_{0.95}Pu_{0.05})C_{0.98}$. 600×. Etchant: nitric acid-acetic acid-water.

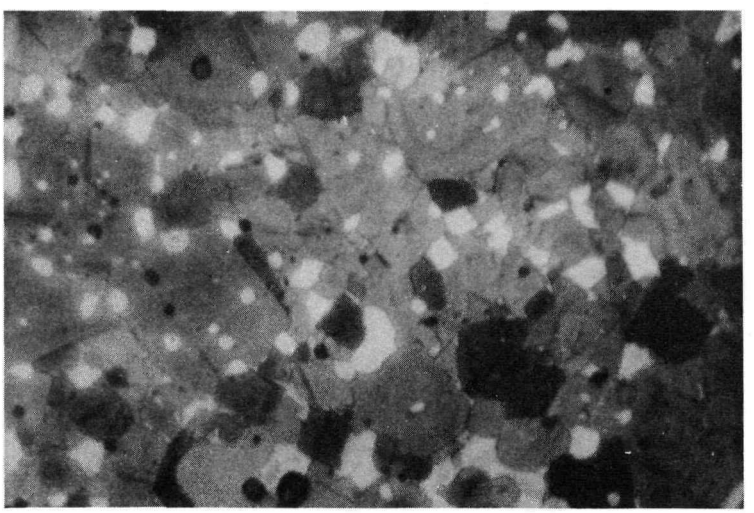

Fig. 4 — Typical structure of $(U_{0.95}Pu_{0.05})C_{0.98}$ + 0.1 w/o Ni. 600×. Etchant: nitric acid-acetic acid-water.

subsequently surface ground to size. Results of these experiments are shown in Table 6.

Metallographic examination showed structures similar to those shown in Figs. 3 and 4.

3.2.2 Fabrication of $(U_{0.8}Pu_{0.2})_2C_3$ Pellets

Several sintering experiments were performed with the 25-g batch of sesquicarbide powder described in Section 3.1.2. For this purpose, the pulverized product was milled for 24 hr in a rubber-lined mill using stainless steel balls.

Pellets for the initial sintering experiment were cold pressed without a binder. The resulting pellets were laminated badly after sintering. Pellets fabricated for subsequent sintering experiments were made with 1/4 w/o Carbowax binder and cold pressed in the usual manner at 30,000 psi. The pellets were 0.225 in. in diameter and about 0.2 in. long. Three experiments were carried out with these pellets. The sintering temperatures were 1650, 1700, and 1750°C with hold times of 1 hr. The results are shown in Table 7.

The cause for the shattering of the pellet during the 1750°C sintering is not known. Similar shattering has been reported for Pu_2C_3 by other investigators. The structure of the 1750°C sintered pellet is shown in Fig. 5.

3.3 VACUUM ANNEALING EXPERIMENTS

The effect of vacuum annealing on structure and composition of $(U_{0.8}Pu_{0.2})C_{0.95}$ was studied with the following objectives.

1. Reacting the residual oxygen (2000 to 4000 ppm) with the carbide
   In addition to lowering the oxygen level, this could produce further densification by producing some free U and Pu which would act as a sintering aid, and then evaporate at the higher temperatures.

Table 6 — Results of Sintering Experiments With $(U_{0.95}Pu_{0.05})C_{0.98}$ Bars

(Bars for Thermal Expansion Studies)

Intended Composition	Sintering Temp, °C	Hold Time, hr	Bar Density, g/cm^3 (Two Bars)	Plutonium,* %	Total Carbon,† w/o	Nitrogen, ppm	X-Ray Analysis
$(U_{0.95}Pu_{0.05})C_{0.98}$	1925	1	11.80-11.81	4.6	4.67	251	Single-phase (UPu)C $a_0 = 4.9607 \pm 0.0003$ Å
$(U_{0.95}Pu_{0.05})C_{0.95}$ plus 0.12 w/o Ni	1550	1	13.17-13.29	5.1	4.77	272	Single-phase (UPu)C $a_0 = 4.962 \pm 0.001$ Å

*Intended plutonium content: 4.75%.
†Intended carbon content: 4.70 w/o.

Table 7 — Results of Sintering Experiments With $(U_{0.8}Pu_{0.2})_2C_3$

Experiment No.	Sintering Temp, °C	Time, hr	Sintered Density*	Total Carbon† w/o	X-Ray Analysis
1	1650	1	11.80-11.90 (11.83 avg)	6.84	Major $(UPu)_2C_3$ Faint (UPu)C
2	1700	1	11.95-12.05 (12.00 avg)	6.75	Major $(UPu)_2C_3$ Faint (UPu)C
3	1750	1	Pellet shattered	6.90	<u>Camera</u> Major $(UPu)_2C_3$ Faint (UPu)C $a_0 = 8.089 \pm 0.004$ Å <u>Diffractometer</u> Major $(UPu)_2C_3$ $a_0 = 8.08997 + 0.00009$ Å -0.00006 Å Moderate (UPu)C $a_0 = 4.959 \pm 0.002$ Å Weak/moderate $(UPu)C_2$

*Theoretical density for Pu_2C_3 is 12.7 g/cm^3 and 12.68 g/cm^3 for U_2C_3.
†Theoretical carbon content is 7.02 w/o.

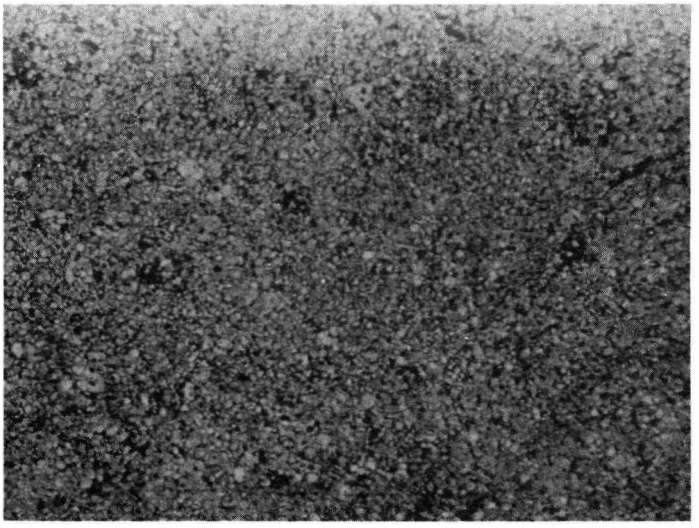

150×

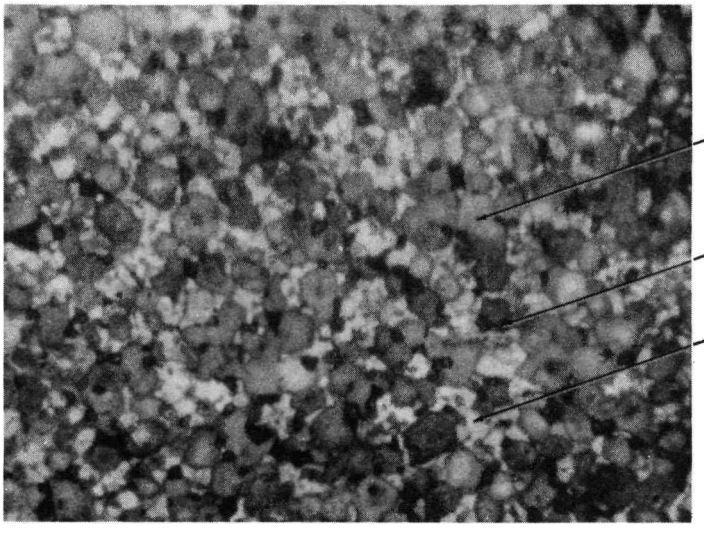

600×

Fig. 5 — Solid solution sesquicarbide $(U_{0.8}Pu_{0.2})_2C_3$. Pellet sintered at 1750°C, 1 hr. Etchant: nitric acid-lactic acid-water.

2. Evaporating the nickel sintering aid

Since the addition of nickel promotes the presence of the sesquicarbide phase, the removal of nickel may transform the material into a single-phase structure.

Preliminary experiments show that the two-phase material (made with nickel sintering aid) can be converted to single-phase material by high temperature vacuum annealing.

The initial vacuum heating cycles decided upon were 1900°C for 1 hr and 2200°C for 1/2 hr. To test objectives (1) and (2), materials without nickel and with 0.1 w/o nickel were run at the above conditions. The changes in dimensions, weights, and bulk densities are summarized in Table 8 together with the observed microstructural changes. The photomicrographs of the unannealed and annealed materials are shown in Figs. 6 through 10.

Fig. 6 shows the structure of a representative sample of $(U_{0.8}Pu_{0.2})C_{0.95}$ + 0.1 w/o Ni before annealing. The white areas are the sesquicarbide phase. After a 1-hr anneal at 1900°C (Fig. 7), the sesquicarbide phase has disappeared and a grain boundary metal phase has formed. Some dicarbide is also evident. When the as-sintered specimen is annealed at 2200°C for 1/2 hr (Fig. 8), a single-phase (UPu)C structure is obtained. The grain boundary metal phase has evaporated and the excess oxygen has apparently accumulated into bubbles, probably as CO, with a subsequent decrease in bulk density. The nickel content has been reduced substantially by the vacuum annealing treatment, from ~1200 to ~100 ppm. Longer hold times may be necessary to reduce the oxygen content as hypothesized above.

Fig. 9 shows the structure of $(U_{0.8}Pu_{0.2})C_{0.95}$ before annealing. No appreciable changes in structure, weight, measurements, or density were found after annealing at 1900°C. However, after the anneal to 2200°C (Fig. 10), the Widmanstätten structure (dicarbide) has disappeared and single-phase material is obtained. A

Table 8 — Effect of Vacuum Annealing on $(U_{0.8}Pu_{0.2})C_{0.95}$ Pellets Previously Sintered in Helium

Sintering Aid	Vacuum Treatment, (~10^{-4} mm Hg)	Weight Change, %	Diameter Change, in.	Bulk Density Change, %	Microstructure Change
0.1 w/o Ni	1900°C, 1 hr	-0.25	+0.0020	-3.2	Sesquicarbide phase gone. Metal grain boundary phase formed. Some "dicarbide" formed.
0.1 w/o Ni	2200°C, 1/2 hr	-1.1	-0.0033	-6.9	Single-phase material obtained. No evidence of grain boundary phase or "dicarbide" seen. Porosity is increased.
No Ni	1900°C, 1 hr	-0.09	+0.0001	-0.40	No significant change. "Dicarbide" phase still present.
No Ni	2200°C, 1/2 hr	-1.0	-0.0011	+0.77	"Dicarbide" phase gone. Single-phase material obtained.

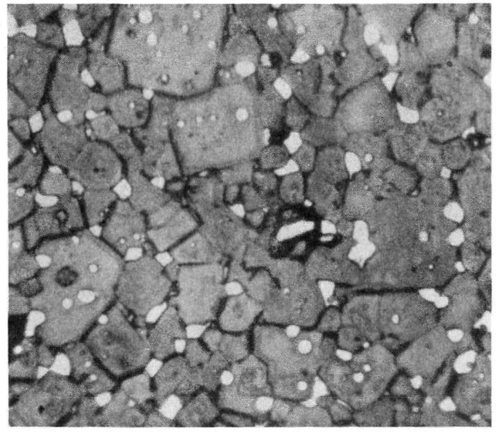

O: ~4000 ppm
Ni: ~1200 ppm
C: 4.6/4.7 w/o

Fig. 6 — $(U_{0.8}Pu_{0.2})C_{0.95}$ + 0.1 w/o Ni – as sintered in helium at 1550°C, 1/2 hr. 600×. Etchant: nitric acid-acetic acid-water.

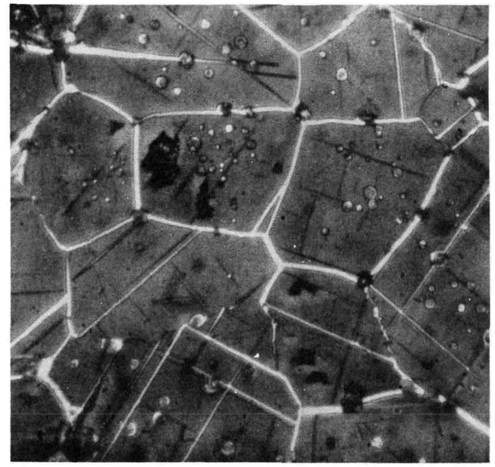

O: ~3600 ppm
Ni: ~140 ppm

Fig. 7 — $(U_{0.8}Pu_{0.2})C_{0.95}$ + 0.1 w/o Ni – sintered in helium and vacuum annealed at 1900°C, 1 hr. 600×. Etchant: nitric acid-acetic acid-water.

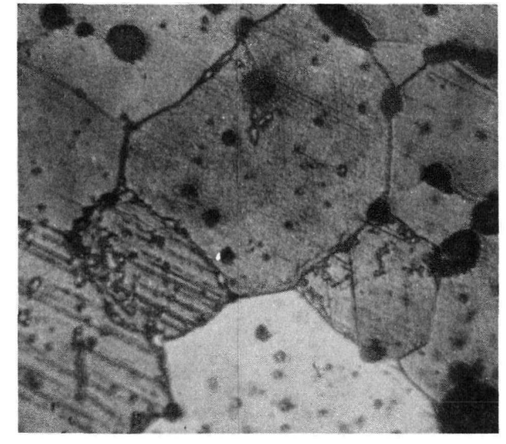

O: ~1600 ppm
Ni: ~100 ppm

Fig. 8 — $(U_{0.8}Pu_{0.2})C_{0.95}$ + 0.1 w/o Ni – sintered in helium and vacuum annealed at 2200°C, 1/2 hr. 600×. Etchant: nitric acid-acetic acid-water.

O: ~2000 ppm

Fig. 9 — $(U_{0.8}Pu_{0.2})C_{0.95}$ – as sintered in helium at 1925°C, 1 hr. 600×. Etchant: nitric acid-acetic acid-water.

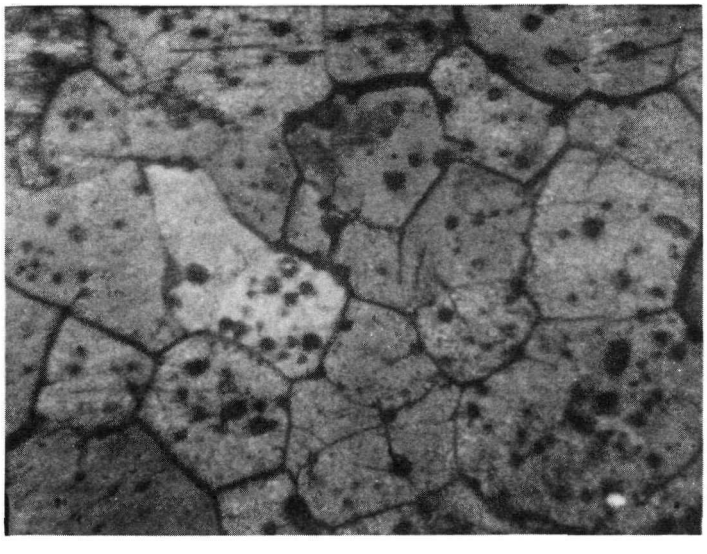

0: ~1000 ppm

Fig. 10 — $(U_{0.8}Pu_{0.2})C_{0.95}$ – sintered in helium and vacuum annealed at 2200°C, 1/2 hr. 600×. Etchant: nitric acid-acetic acid-water.

slight density increase was obtained, perhaps indicating that some liquid-phase sintering had occurred as hypothesized in (1) above. The oxygen content was reduced by one-half in agreement with the hypothesis. However, further study is needed.

3.4 EFFECT OF AGING ON LATTICE PARAMETERS

Studies at Harwell and Hanford have shown that the lattice parameter of plutonium compounds increases with time. The reason for the parameter increase was postulated as an alpha radiation effect.

A change in lattice parameter with time would be significant in the identification of plutonium compounds; therefore, a study was initiated to determine the effect on $(U_{0.95}Pu_{0.05})C_{0.98}$ and $(U_{0.8}Pu_{0.2})C_{0.95}$. The results to date are shown in Tables 9 and 10.

A general slight increase in lattice parameter can be noted; but, considering the accuracy of the measurements, the increase is not significant. Self-damage due to alpha radiation should be more pronounced with the higher plutonium composition (Table 10); however, this was not evident.

3.5 MICROPROBE ANALYSES

Microprobe analyses were completed to identify phases by chemical composition, and to determine the uniformity of distribution of plutonium and nickel. The analyses were carried out by the Monsanto Research Corporation's Mound Laboratory on an ARL electron-beam microprobe X-ray analyzer.

Previous analyses of $(U_{0.8}Pu_{0.2})C_{0.95}$ + 0.1 w/o Ni (See UNC-5055, Section 3.4.3) concluded that nickel was concentrated at the grain boundaries. Relative uranium and plutonium contents were obtained, but absolute contents could not be determined because of insufficient standards. The standards used to that date were uranium metal, UC, and nickel.

Table 9 — Effect of Aging on Lattice Parameter of $(U_{0.95}Pu_{0.05})C_{0.98}$ Powder (Camera Method)

Date	Phase Present	Unit Cell Size
12/15/62	Single-phase (UPu)C	$a_0 = 4.9607 \pm 0.0003$ Å
1/15/63	Single-phase (UPu)C	$a_0 = 4.9603 \pm 0.0004$ Å
2/15/63	Single-phase (UPu)C	$a_0 = 4.9612 \pm 0.0005$ Å
3/15/63	Single-phase (UPu)C	$a_0 = 4.9613 \pm 0.0009$ Å
4/15/63	Single-phase (UPu)C	$a_0 = 4.960 \pm 0.001$ Å

Table 10 — Effect of Aging on the Lattice Parameter of $(U_{0.8}Pu_{0.2})C_{0.95}$ Powder (Diffractometer Method)

Date	Phases Present	Unit Cell Size
4/15/63	Major (UPu)C Weak $(UPu)C_2$ Faint $(UPu)_2C_3$	$a_0 = 4.9648 \pm 0.0005$ Å
5/15/63	Major (UPu)C Faint $(UPu)_2C_3$ and $(UPu)C_2$	$a_0 = 4.9661 \pm 0.0003$ Å
6/23/63	Major (UPu)C Faint $(UPu)_2C_3$ and $(UPu)C_2$	$a_0 = 4.9667 \pm 0.0007$ Å
11/8/63	Major (UPu)C Faint $(UPu)_2C_3$ and $(UPu)C_2$	$a_0 = 4.9666 \pm 0.0004$ Å

Arc-cast PuC and Pu_2C_3 were prepared by General Electric Company's Hanford Laboratories. Although each of the standards was a mixture of PuC and Pu_2C_3, the phases were large enough in area to be used as standards. Additional standards used were UC, UC + 0.1 w/o Ni (which contains U_2C_3), and nickel.

The following conclusions were drawn from the results.

1. The plutonium and nickel uniformity in the samples is better than the sensitivity of the instrument (with the possible exception of one indication that nickel is not concentrated at the grain boundaries)
2. The plutonium to uranium ratio in the "sesquicarbide" phase is higher than in the monocarbide phase, assuming the monocarbide phase has a Pu/U ratio of 2/8, the sesquicarbide phase would have a Pu/U ratio of 3.63/6.37
3. Absolute plutonium and uranium analyses were hindered by surface film formations on the highly oxidizable carbides.

3.6 FUEL CLAD COMPATIBILITY

The compatibility of $(U_{0.8}Pu_{0.2})C_{0.95}$ with potential cladding materials was studied under conditions similar to those that would prevail in a fuel element. Fuel and cladding materials were held in contact with each other in capsules similar to the one shown in Fig. 11. Continued contact between fuel and cladding samples at elevated temperatures was assured by the greater thermal expansion of the stainless steel insert compared to the Inconel container. Most of the capsules contained duplicates of the same cladding materials. The capsules were seal-welded in a glove box containing a helium atmosphere, decontaminated, leak-checked, taken out of the glove box line, and placed in the sealed inner shell of the furnaces. The furnaces stood in a hood in the Plutonium Facility.

Metallographic examination, subsequent to the tests, determined the degree of interaction between fuel and cladding samples.

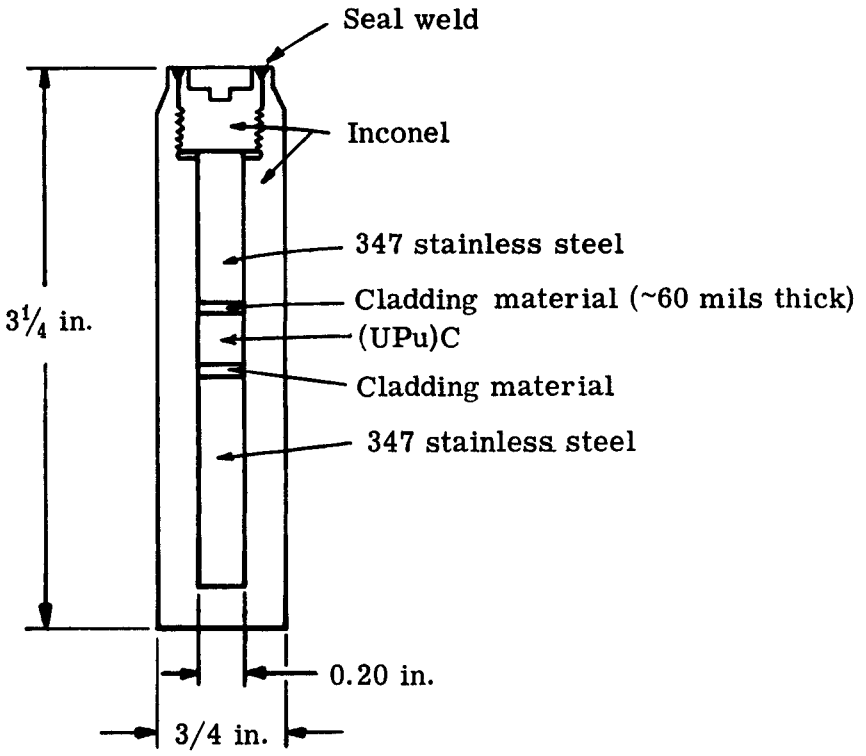

Fig. 11 — Compatibility capsule

Fuel

The fuel samples used are described in Section 3.2.1. All the samples were hypostoichiometric in carbon content, but had sufficient oxygen in solid solution to produce microstructures with higher carbides and no free metal. Typical structures are shown in Figs. 3 and 4.

Type 316 Stainless Steel

There were no reactions between fuel and type 316 stainless steel samples, as shown in Table 11. Typical samples of steel which had been in contact with fuel are shown in Fig. 12. The carbide and sigma precipitation in the steel are a thermal effect, and not a product of interaction with the fuel.

Table 11 — Fuel-Type 316 Stainless Steel Compatibility

Fuel	Temperature, °C (°F)	Time, hr	Remarks
$(U_{0.95}Pu_{0.05})C_{0.98}$	593 (1100)	4000	No reaction
$(U_{0.95}Pu_{0.05})C_{0.98}$ + 0.1 w/o Ni	593	4000	No reaction
$(U_{0.95}Pu_{0.05})C_{0.98}$	816 (1500)	1000	No reaction
$(U_{0.95}Pu_{0.05})C_{0.98}$ + 0.1 w/o Ni	816	1000	No reaction
$(U_{0.95}Pu_{0.05})C_{0.98}$	816	4000	No reaction
$(U_{0.95}Pu_{0.05})C_{0.98}$ + 0.1 w/o Ni	816	4000	No reaction (Fig. 12)

2¼ Cr-1 Mo Steel

There were no reactions between fuel and 2¼ Cr-1 Mo steel, as shown in Table 12.

A typical sample of steel which had been in contact with fuel is shown in Fig. 13. Considerable grain growth occurred at the higher test temperature, as would be expected.

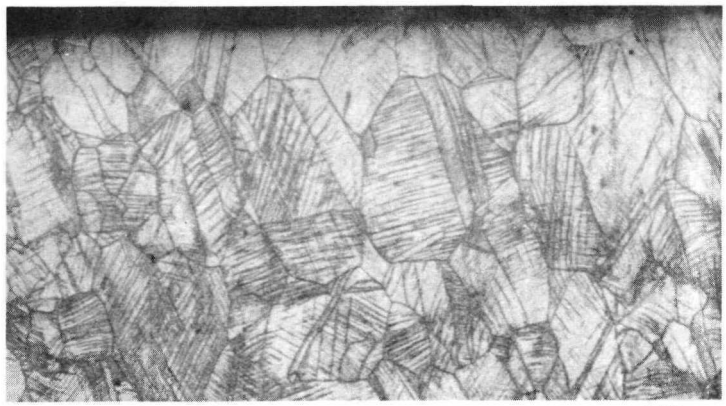

Glyceregia etch 150 ×

From test with $(U_{0.95}Pu_{0.05})C_{0.98}$ for 4000 hr at 593°C (1100°F)

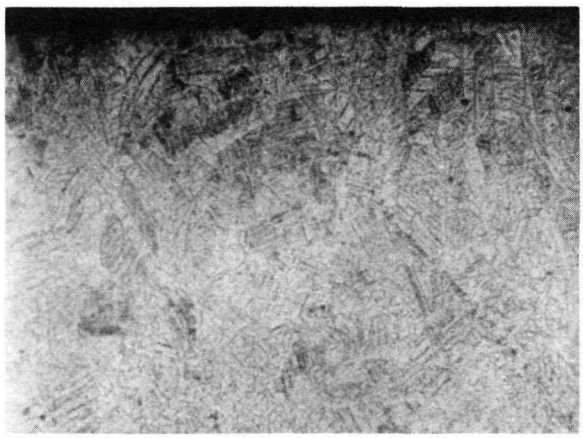

Glyceregia etch 100 ×

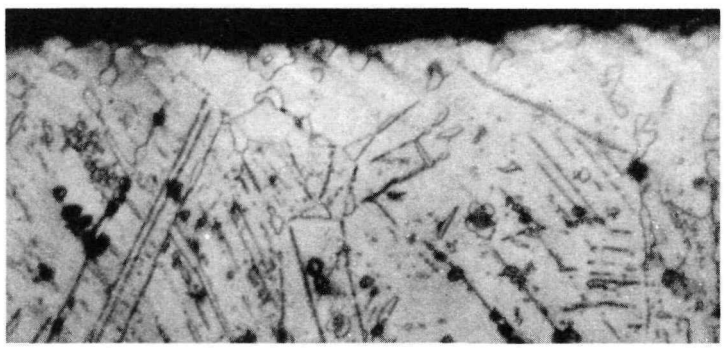

Glyceregia etch 600 ×

From test with $(U_{0.95}Pu_{0.05})C_{0.98}$ for 4000 hr at 816°C (1500°F)

Fig. 12 — Type 316 stainless steel from compatibility test

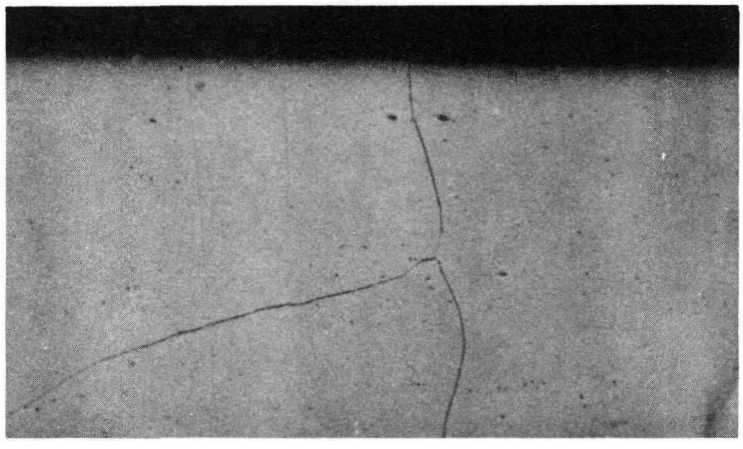

Nital etch 150×

From test with $(U_{0.95}Pu_{0.05})C_{0.98}$ for 4000 hr at 816°C (1500°F)

Fig. 13 — $2\frac{1}{4}$ Cr-1 Mo steel from compatibility test

Table 12 — Fuel-$2\frac{1}{4}$ Cr-1 Mo Steel Compatibility

Fuel	Temperature, °C (°F)	Time, hr	Remarks
$(U_{0.95}Pu_{0.05})C_{0.98}$	593 (1100)	4000	No reaction
$(U_{0.95}Pu_{0.05})C_{0.98}$ + 0.1 w/o Ni	593	4000	No reaction
$(U_{0.95}Pu_{0.05})C_{0.98}$	816 (1500)	4000	No reaction

Niobium, Niobium-1 w/o Zirconium

There were no reactions between fuel and niobium, or niobium-1 w/o zirconium alloy with the exception of one case, as shown in Table 13. A typical niobium sample which was in contact with fuel and did not react is shown in Fig. 14. Typical niobium-1 w/o zirconium samples that were in contact with the fuel are shown in Fig. 15. One of the samples reacted slightly with the fuel. The reaction layer is an average of 0.008 mm (0.0003 in.) thick. Its composition was not identified. The niobium was annealed by the test temperature, whereas the niobium-1 w/o zirconium was not.

Zircaloy-2

A reaction was noted between $(U_{0.8}Pu_{0.2})C_{0.95}$ and Zircaloy-2 in 1000 hr at 593 and 816°C. Fig. 16 shows a typical Zircaloy-2 interface with the fuel. The reaction product has not been identified.

3.7 COEFFICIENT OF THERMAL EXPANSION MEASUREMENTS

The coefficient of thermal expansion was determined from room temperature to 1400°C in vacuum for sintered $(U_{0.95}Pu_{0.05})C_{0.98}$ with and without nickel sintering aid. The presence of the sintering aid did not affect the coefficient of expansion significantly. The values obtained for the mixed uranium-plutonium carbides are about 5% higher than the literature values given for UC. The results of this in-

Table 13 — Fuel-Niobium, Niobium-1% Zirconium Compatibility

Fuel	Clad	Temperature, °C (°F)	Time, hr	Remarks
$(U_{0.95}Pu_{0.05})C_{0.98}$	Nb	593 (1100)	4000	No reaction
	Nb-1% Zr			No reaction
$(U_{0.95}Pu_{0.05})C_{0.98}$ + 0.1 w/o Ni	Nb	593	4000	No reaction
	Nb-1% Zr			No reaction
$(U_{0.95}Pu_{0.05})C_{0.98}$	Nb	816 (1500)	1000	No reaction
	Nb-1% Zr			No reaction
$(U_{0.95}Pu_{0.05})C_{0.98}$ + 0.1 w/o Ni	Nb	816	1000	No reaction
	Nb-1% Zr			No reaction
$(U_{0.95}Pu_{0.05})C_{0.98}$	Nb	816	4000	No reaction (Fig. 14)
	Nb-1% Zr			Reaction noted (Fig. 15)
$(U_{0.95}Pu_{0.05})C_{0.98}$ + 0.1 w/o Ni	Nb	816	4000	No reaction
	Nb-1% Zr			No reaction (Fig. 15)

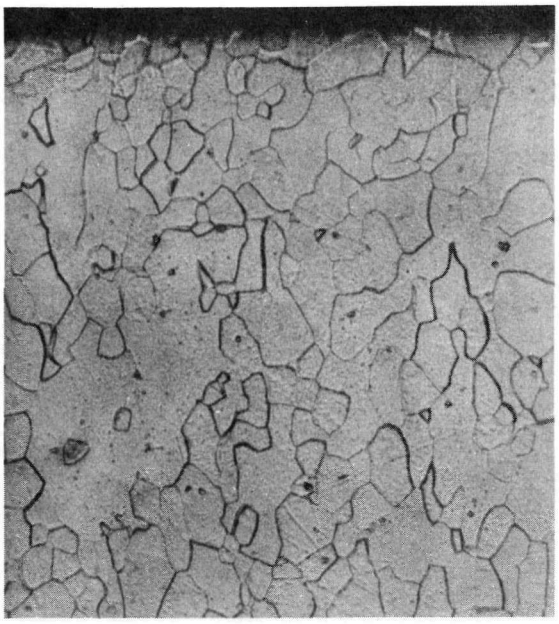

150 ×

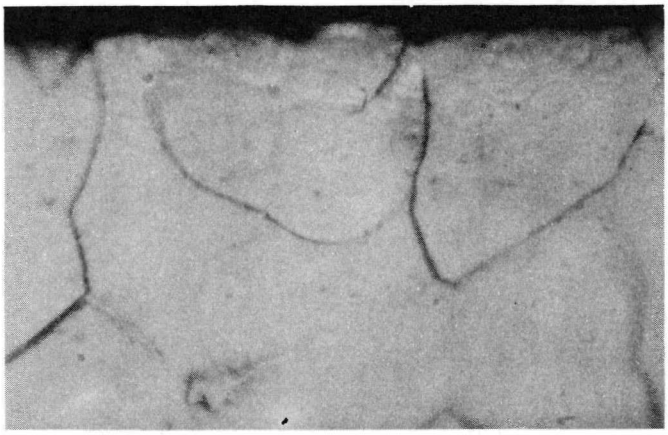

600 ×

From test with $(U_{0.95}Pu_{0.05})C_{0.98}$ for 4000 hr at 816°C (1500°F)

Fig. 14 — Niobium from compatibility test

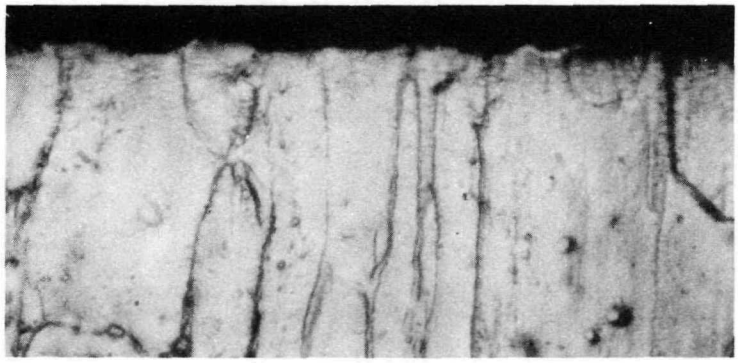

600 ×

From test with $(U_{0.95}Pu_{0.05})C_{0.98}$ + 0.1 w/o Ni for 4000 hr at 816°C (1500°F)

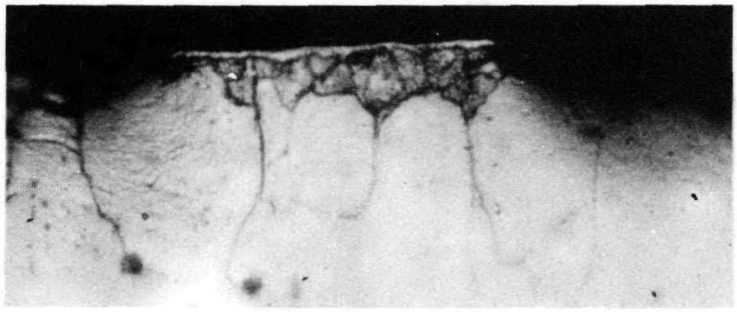

600 ×

From test with $(U_{0.95}Pu_{0.05})C_{0.98}$ for 4000 hr at 816°C (1500°F). Reaction layer is 0.0003 in., average.

Fig. 15 — Niobium-1% zirconium from compatibility test

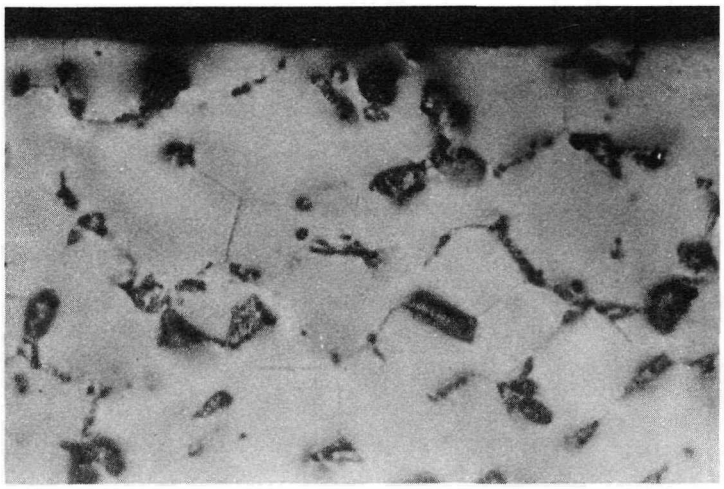

150 ×

From test with $(U_{0.95}Pu_{0.05})C_{0.98}$ for 1000 hr at 816°C (1500°F)

Fig. 16 — Zircaloy-2 from compatibility test

vestigation are in general agreement with those of other investigators. The comparison is made in Table 14.

The detailed data for $(U_{0.95}Pu_{0.05})C_{0.98}$ are given in Tables 15 and 16 and include the results of two heating and cooling runs for each specimen. The accuracy of the values is about ±5%. The expansion curves were smooth, and did not show any transformations.

The thermal expansion of arc-cast uranium carbide was measured from room temperature to 1360°C. This material was chosen to provide experimental data checks of the dilatometer on a material with a coefficient of expansion likely to be similar to (UPu)C. The calculated data given in Table 17 are in fair agreement with the literature values.

The coefficients were determined with a differential dilatometer consisting of high purity, high density, tubular alumina elements (Fig. 17). The difference in expansion between the alumina and the specimen was sensed by both a dial gage and a linear transformer. These differences were plotted against temperature. Since the carbide specimens expand more than the alumina dilatometer tube, these data points are added to the expansion curve for alumina to obtain the true expansion of the specimen. A smooth curve was then drawn through the points and the coefficients of thermal expansion were calculated.

Prior to the testing of carbides, a tantalum standard was tested in vacuum, to 1485°C, to obtain a calibration curve for the alumina dilatometer. The curve obtained for alumina checked those of previous investigators within ±7%. The spread of values for alumina among previous investigators is ±3%.

The nominal specimen size was 0.2 in. by 0.3 in. by 2.0 in. long. No appreciable changes in dimensions were found after testing of the specimens. In addition, no appreciable changes in structure or composition of the test specimens were noted, as shown in Table 18.

Table 14 — Summary of Carbide Thermal Expansion Coefficients

Material	Source	Temperature Range, °C	Coefficient, 10^{-6}/°C
Sintered UC	Taylor (Carborundum Co.)	25-950	11.2
Sintered UC	Crane (United Nuclear)	25-950	11.4
Cast UC	Crane (United Nuclear)	25-950	11.6
Cast UC	Secrest (BMI)	25-950	11.4
Cast $(U_{0.87}Pu_{0.13})C$	Ogard (LA)	25-900	11.1
Cast $(U_{0.85}Pu_{0.15})C$	(Harwell)	25-1000	11.1-11.8
Sintered $(U_{0.85}Pu_{0.15})C$	(Harwell)	25-1000	11.1
Hot Pressed $(U_{0.85}Pu_{0.15})C$	(Harwell)	25-1000	10.8
Sintered $(U_{0.8}Pu_{0.2})C_{0.95}$	Stahl (United Nuclear)	25-950	11.3
		25-1400	11.9
Sintered $(U_{0.8}Pu_{0.2})C_{0.95}$ + 0.1 w/o Ni	Stahl (United Nuclear)	25-950	11.4
		25-1400	12.3
Sintered $(U_{0.95}Pu_{0.05})C_{0.98}$	Stahl (United Nuclear)	25-1000	12.0
		25-1400	12.6
Sintered $(U_{0.95}Pu_{0.05})C_{0.98}$ + 0.1 w/o Ni	Stahl (United Nuclear)	25-1000	11.8
		25-1400	12.2

Table 15 — Coefficient of Expansion of $(U_{0.95}Pu_{0.05})C_{0.98}$

Thermal Expansion Coefficients, $10^{-6}/°C$

Temperature Range, °C	Transformer First Heating	Transformer First Cooling	Transformer Second Heating	Dial Gage First Heating	Dial Gage First Cooling	Dial Gage Second Heating	Overall Value (all runs)
25-200	9.42	8.58	8.29	8.68	9.70	9.43	9.0
25-400	10.4	10.4	9.20	9.75	10.7	10.0	10.0
25-600	11.1	11.5	10.3	10.6	11.7	10.8	10.8
25-800	11.7	12.1	11.2	11.4	12.4	11.6	11.6
25-1000	12.2	12.5	11.8	11.7	12.8	12.1	12.0
25-1200	12.7	12.7	12.2*	12.2	13.0	12.4*	12.4
25-1400	13.1	12.9	12.4	12.5	13.3	12.6	12.6

*Interpolated.

Table 16 — Coefficient of Expansion of $(U_{0.95}Pu_{0.05})C_{0.98}$ + 0.1 w/o Ni

Thermal Expansion Coefficients, $10^{-6}/°C$

Temperature Range, °C	Transformer First Heating	Transformer First Cooling	Transformer Second Heating	Dial Gage First Heating	Dial Gage First Cooling	Dial Gage Second Heating	Overall Value (all runs)
25-200	8.58	7.55	8.87	9.15	9.71	8.30	8.60
25-400	10.9	8.75	9.86	10.2	10.7	9.20	10.2
25-600	11.7	9.73	10.8	10.8	11.7	10.1	10.9
25-800	12.0	10.7	11.3	11.4	12.3	10.8	11.4
25-1000	12.2	11.7	11.7	12.0	12.9	11.3	11.8
25-1200	12.2	12.4	11.9	12.1	13.4	11.6	12.1
25-1400	12.2	12.5	12.1	12.2	13.4	11.7	12.2

Table 17 — Coefficient of Expansion of Arc-Cast UC

Temperature Range, °C	Coefficient of Thermal Expansion, 10^{-6}/°C								
	Transformer			Dial Gage					
	First Heating	Second Heating	First Cooling	First Heating	Second Heating	First Cooling	Third Heating	Overall Value	Crane (UNC)*
30-200	8.30	10.7	9.11	9.30	10.0	11.7	8.83	9.70	10.2
30-400	9.7	11.3	10.0	10.2	11.4	12.3	10.3	10.7	10.8
30-600	10.7	12.3	11.0	11.6	12.0	12.7	11.8	11.7	11.1
30-800	12.0	13.0	11.8	12.7	12.3	13.0	12.3	12.4	11.4
30-1000	12.9	13.4	12.2	13.6	12.6	13.3	12.8	12.8	11.6
30-1200	-	13.7	12.4	-	12.6	13.5	13.1	13.0	-
30-1360	-	13.8	12.6	-	12.7	13.7	-	13.2	-

*Preliminary data on similar material.

Table 18 — Analysis of Thermal Expansion Bars

Item	Condition	$(U_{0.95}Pu_{0.5})C_{0.98}$	$(U_{0.95}Pu_{0.05})C_{0.98}$ + 0.1 w/o Ni
Carbon, w/o			
UNC	Untested	4.69	4.81
Carborundum	Untested	4.67	4.77
Carbon, w/o			
UNC	Tested	4.67	4.83
Plutonium, w/o	Untested	4.99	5.10
Plutonium, w/o	Tested	5.01	4.95
Metallography	Untested	Single-phase (UPu)C	Major phase (UPu)C Minor phase $(UPu)_2C_3$
Metallography	Tested	Same as Untested	
X-ray (camera method)	Untested	Single-phase (UPu)C a_0=4.9607±0.0003 Å	Single-phase (UPu)C a_0=4.962±0.001 Å

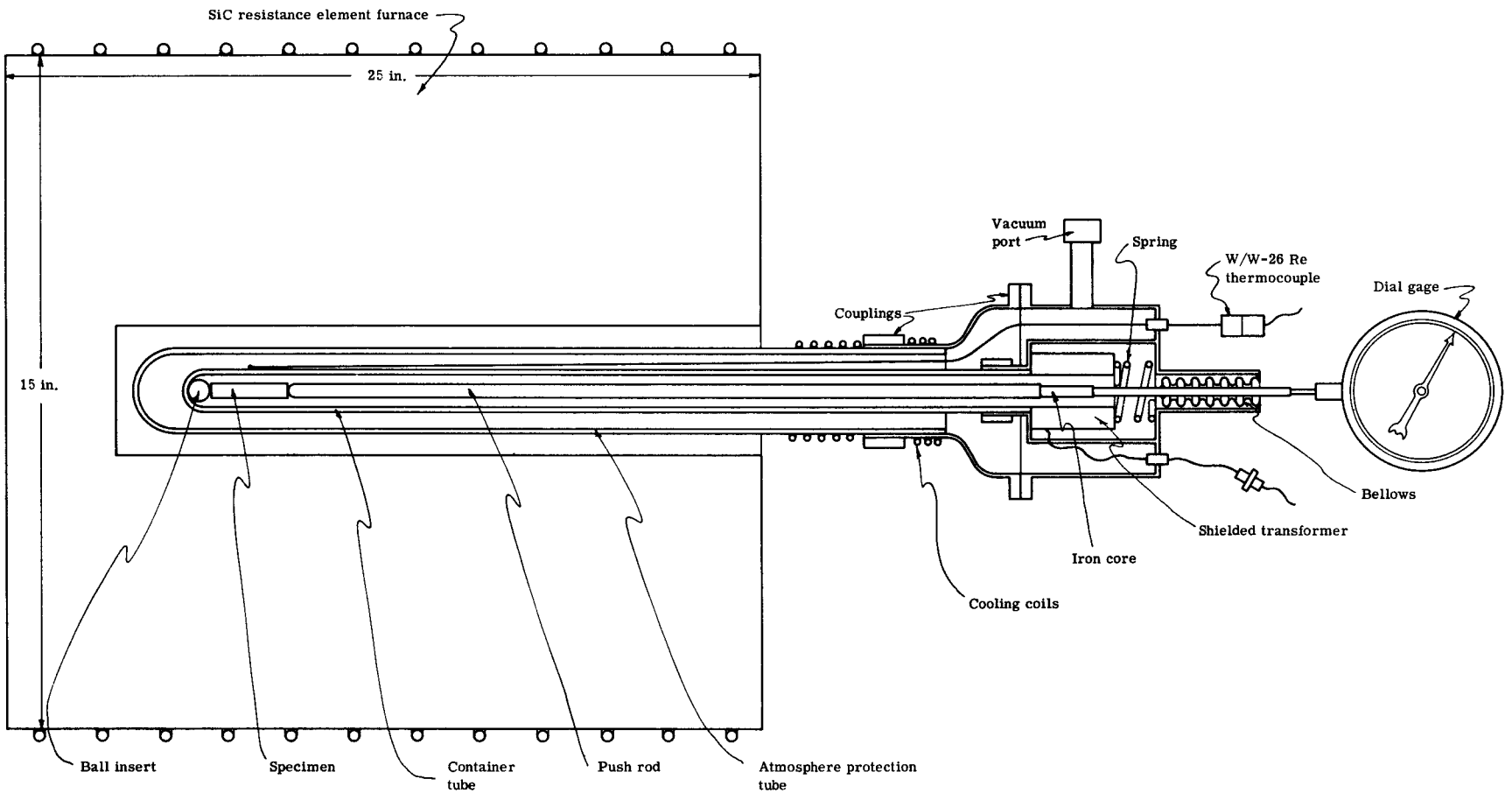

Fig. 17 — Schematic of dilatometer

3.8 MELTING POINT DETERMINATIONS

The melting point measurements of standards were completed and one measurement on $(U_{0.95}Pu_{0.05})C_{0.98}$ gave 2500°C. Additional determinations will be made.

The measurements were made in the tantalum resistance vacuum furnace. The temperature of the specimen was determined with a micro-optical pyrometer. The optical readings were corrected for errors due to absorption in the box window, prism, and sight glass, by melting materials with well known melting points. A calibration curve shown in Fig. 18 was obtained from the observed and accepted melting points.

The cylindrical standard specimens contained black body holes drilled into the top surface. The sides were notched to aid the viewer in observing the actual melting point. The fuel specimens are 0.2 in. diameter by 0.2 in. high, but do not contain a black body hole.

Only one melting point determination has been made to date. A solid fuel pellet was held in an internally carburized tantalum cup. A corrected melting point of 2500°C was obtained.

3.9 VAPOR PRESSURE MEASUREMENTS

3.9.1 Introduction

The objective of the measurements is to obtain the vapor pressure of $(U_{0.95}Pu_{0.05})C_{0.98}$ by the Knudsen method. To date, the vapor pressure of a silver standard was determined to calibrate the system geometry. A modified two-piece Knudsen cell was designed and fabricated out of tantalum, and carburized successfully. Analytical techniques to measure microgram quantities of uranium were developed.

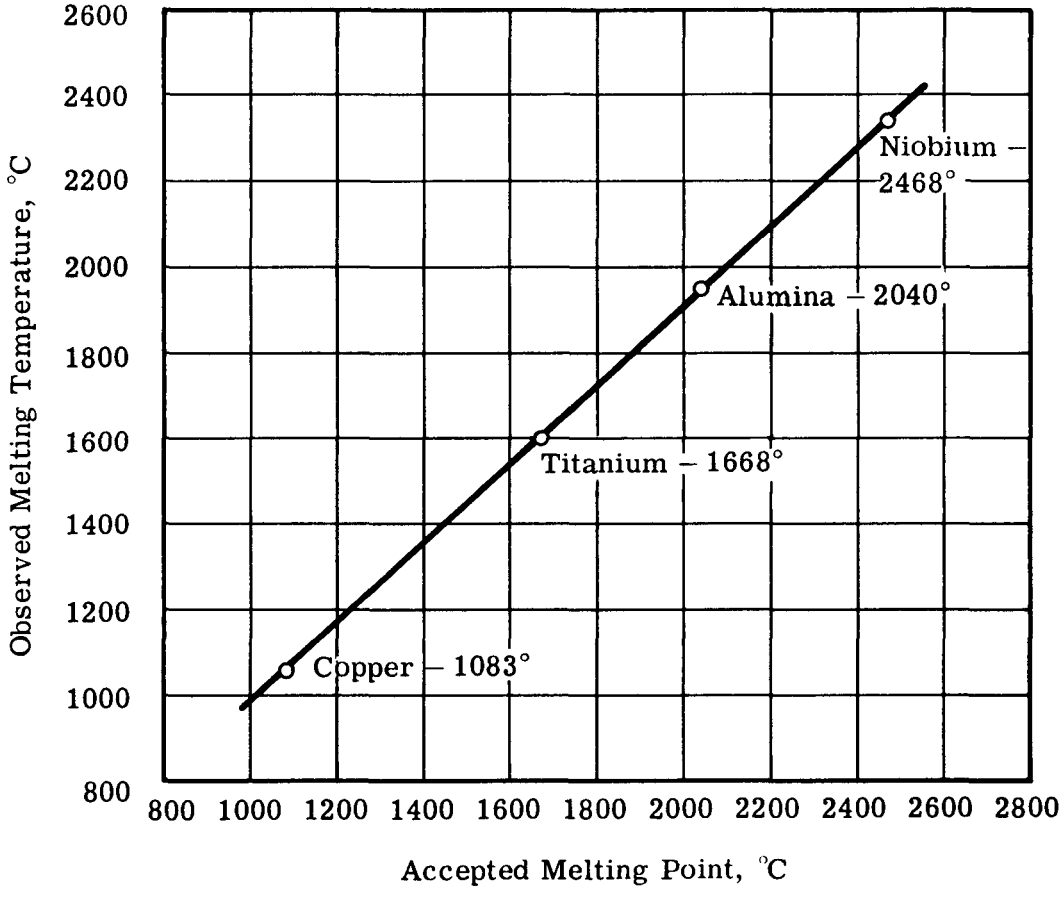

Fig. 18 — Temperature correction curve based on melting of standards

3.9.2 Experimental Equipment

The Knudsen effusion experiment is shown schematically in Fig. 19.

The Knudsen effusion cell is centered in a tubular tantalum heating element standing on a tantalum pedestal.

During the experiment, perforations in the tantalum heat shield collimate a known fraction of the vapor beam which then condenses on a water-cooled counting planchet. Eight planchets, located on a wheel, can be lined up with the vapor beam successively without breaking the vacuum. In practice, a maximum of seven planchets is used so that direct optical pyrometer sighting on the orifice is possible. Swaged commercial W-W/26% Re thermocouples located in the tantalum pedestal under the cell were intended to be used. However, their poor reliability and short lifetime at these temperatures prevented their use to date. An improved, unswaged thermocouple design with insulating beads was completed and is being procured.

3.9.3 Knudsen Cell Design

The cell material must be compatible with the (UPu)C and with the furnace components. An internally carburized tantalum cup was chosen. The carbide inner layer prevents the reaction of (UPu)C with tantalum which would produce free uranium and plutonium and minimizes the amount of interfering tantalum vapor in the cell.

The cell is fabricated in two sections. The bottom section is a cup spun from 0.010-in. thick tantalum sheet to 0.375 in. OD and 1/2 in. high. The cover is also spun from 0.010-in. thick sheet to form a cup 0.355 in. OD by 1/8 in. high. The orifice hole was drilled and the base was machined down to produce an orifice thickness of about 0.002 in., which is small enough to eliminate channeling effects. The small ratio of the hole-to-cell areas assures a vapor pressure near equilibrium in the cell.

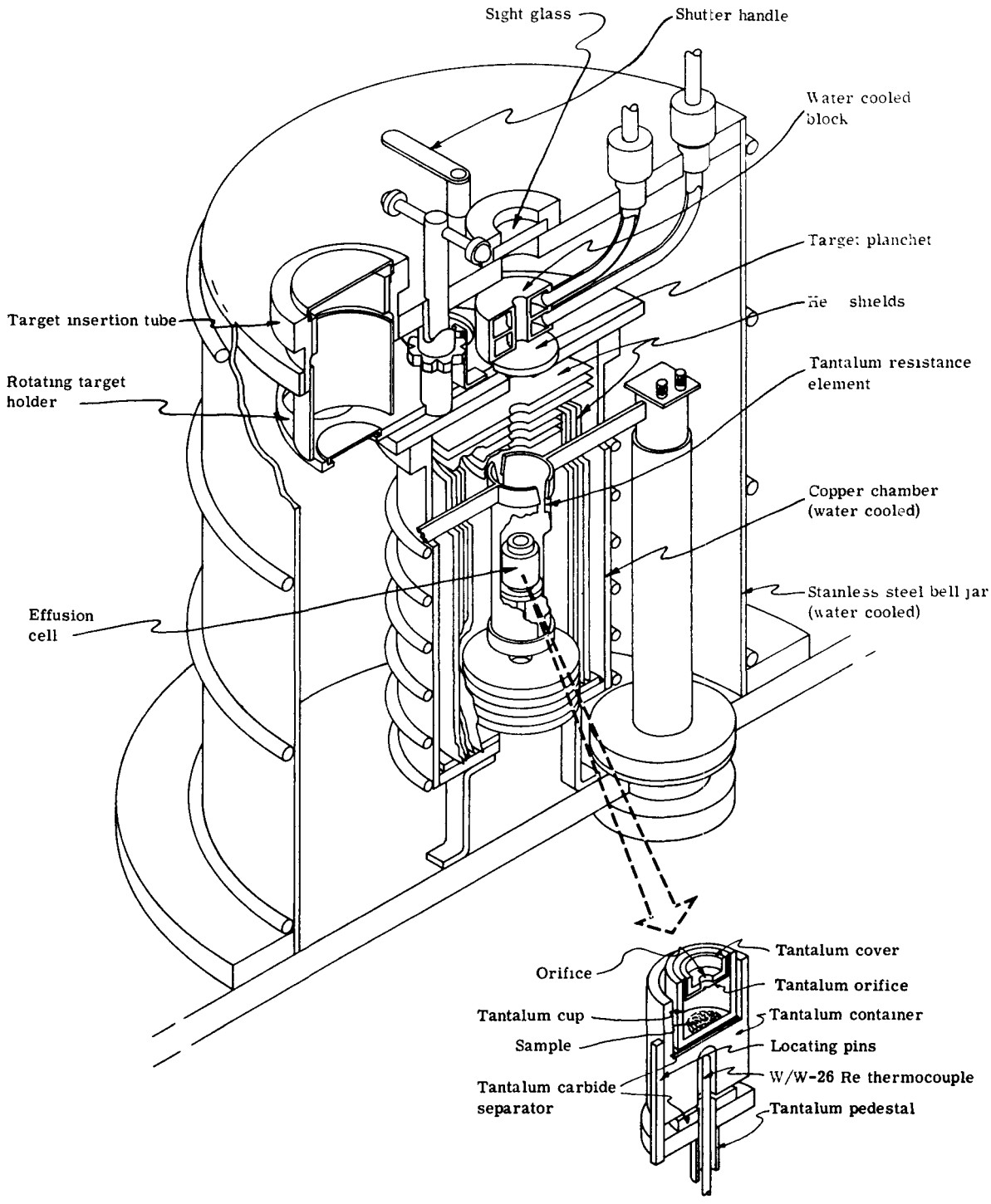

Fig. 19 — Schematic of thermal stability experiment

The cell components are carburized prior to welding. Heating the tantalum cups at ~2000°C for 1 hr in contact with graphite flour produced a continuous 0.003-in. tantalum carbide coating. A carburization cycle of ~1700°C for 1/2 hr was used for the tantalum covers to produce a 0.0005 to 0.0008-in. coating on the 0.0020-in. orificed section. Zones, 1/8-in. max., next to the top edges were left uncarburized for welding. The covers are welded to the cups after the introduction of several hundred mg of test sample.

3.9.4 System Geometry Calibration

The geometry of the collimator and collection system was calibrated with a cell containing high purity (99.999%) silver. The fraction of vapor collected was calculated from a preliminary run at about 1400, 1500, and 1600°K and determined as 0.0224. The results are shown in Table 19. Silver was determined spectrophotometrically using copper dithizonate reagent.

Table 19 — Silver Vapor Pressure Test

Target	Temperature, °K	Time, sec	Accepted Vapor Pressure, mm Hg	Deposit,* μg	Calculated Weight Effused, μg	Fraction Collected
1	1403	2340	5.5×10^{-2}	24.0	1000	0.0240
2	1404	2280	5.5×10^{-2}	21.9	978	0.0224
3	1500	540	2.4×10^{-2}	21.7	979	0.0222
4	1503	540	2.4×10^{-2}	21.9	977	0.0225
5	1600	150	9.0×10^{-2}	23.8	985	0.0241
6	1601	180	9.0×10^{-2}	26.4	1180	0.0224
7	1498	600	2.4×10^{-1}	24.3	1090	0.0224

*Corrected for slight blockage of target.

4. IRRADIATION TESTS

4.1 EXPERIMENT DESIGN AND ASSEMBLY

Twelve clad $(U_{0.8}Pu_{0.2})C_{0.95}$ specimens are being irradiated to determine the effect of power and burnup on the stability of the fuel.

Each irradiation capsule contains two specimens. Each specimen consists of 16 fuel pellets, 0.191 in. diameter, for a 3-in. fueled length. The clad is stainless steel or niobium. Both specimens contain $(U_{0.8}Pu_{0.2})C_{0.95}$, but one was prepared without sintering aid and one was prepared with 0.1 w/o nickel sintering aid. The void space is filled with helium. The cold fuel-clad gap at assembly varied from 0.0005 to 0.0025 in. The specimens, designed to operate at less than 1040°C (1900°F) central fuel temperatures, have a central niobium thermocouple well and for this reason they are also clad with niobium. The higher temperature specimens do not have provision for fuel center temperature measurement. The latter are clad with type 316 stainless steel, because this is potentially one of the most economical fuel clads for a fast reactor, central station, power plant. Cross sectional views of the two types of irradiation specimens are shown in Fig. 20.

The specimens with central thermocouples were used to obtain an estimate of the in-pile thermal conductivity of the fuel.

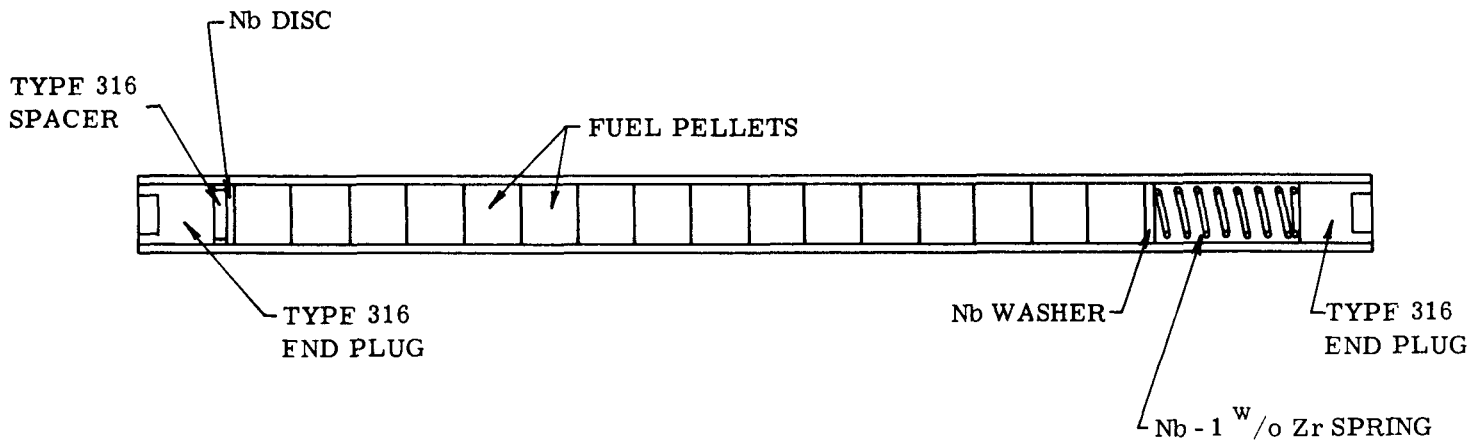

TYPE 316 STAINLESS STEEL CLAD SPECIMEN

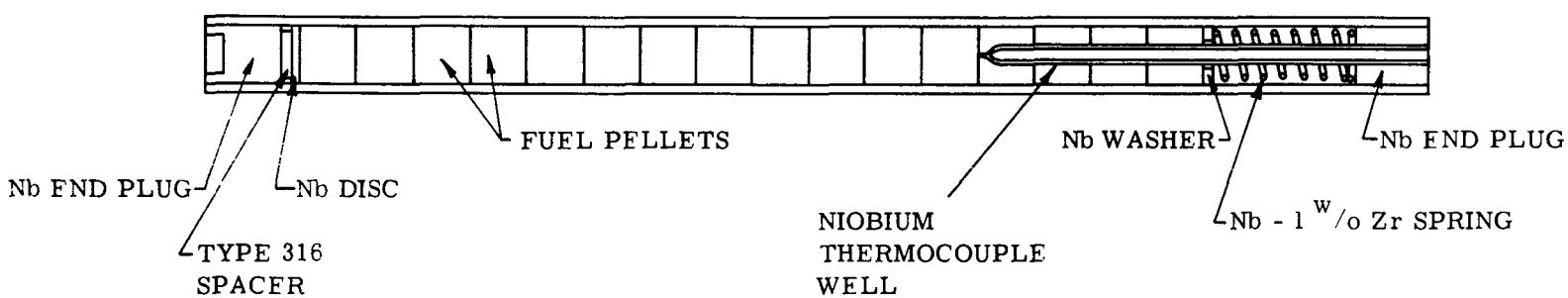

NIOBIUM CLAD SPECIMEN

Fig. 20 — Irradiation specimens – cross sectional view

The fabrication of the fuel and the assembly of the specimens was described in the Phase IV Report, UNC-5055.

The intended irradiation conditions are:

10^{20} fiss/cm^3	(MW-d/T)	Power, max. w/cm	(kw/ft)	Specimen Nos.	Capsule Nos.
~5.6	(~17,000)	490	(15)	61T, 61B	61
		650	(20)	64T, 64B	64
~11.2	(~34,000)	490	(15)	62T, 62B	62
		650	(20)	65T, 65B	65
~22.4	(~68,000)	490	(15)	63T, 63B	63
		650	(20)	66T, 66B	66

Fig. 21 is a cross sectional view of a typical irradiation capsule. The capsule consists of an inner and outer shell. The inner shell contains the specimens along with the thermocouples and electric heaters. Sodium is used to fill the inner shell to serve as the heat transfer medium. Radial fins on the outside of the inner shell are designed to give the proper thermal resistance for the desired temperatures and power levels. The annulus between the inner and outer shell is filled with helium.

The thermocouples are placed in three radial locations: fuel center (lower power capsules only), specimen OD, and the OD of the inner shell. The thermocouple pair at the specimen center and OD were used to measure thermal conductivity. The thermocouple at the fin root, in conjunction with the reactor coolant water temperature, was used to measure the heat generation rate.

The assembly of all experiments was completed during Phase V.

4.2 EXPERIMENT OPERATION

All 12 fuel specimens were inserted and operated in the General Electric Test Reactor (GETR) as close to design temperatures as reactor power fluctuations

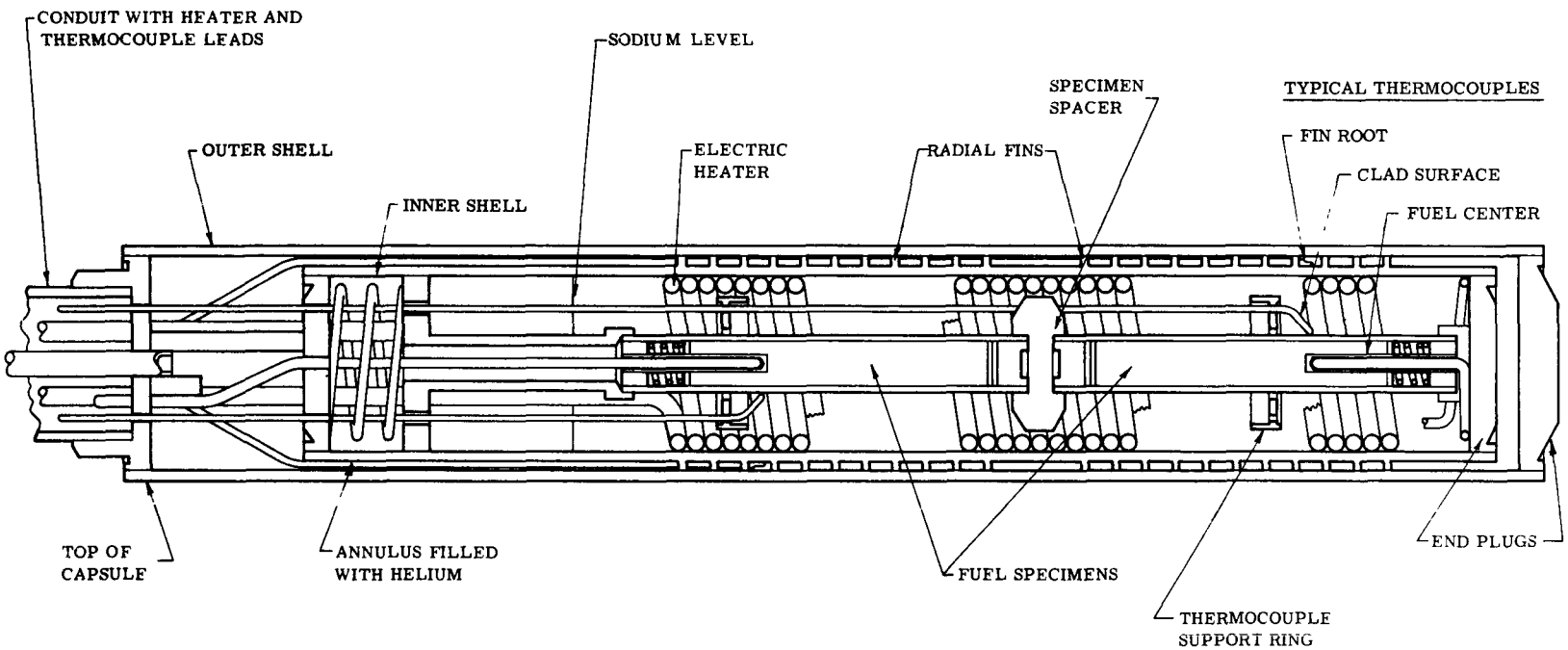

NOTE: FOR CLARITY THE DIAMETER DIMENSIONS HAVE BEEN INCREASED BY A FACTOR OF 2.

Fig. 21 — Irradiation capsule – cross sectional view

would permit. The operating conditions of specimens in Capsules 62, 63, 65, and 66 are summarized in Table 20. Capsule 65, a high power capsule for irradiation in the GETR core, was started up with the April cycle (No. 43). In order to check the heat transfer characteristics of the capsule, initial irradiation was in the pool. The experimentally determined capsule thermal resistances were in good agreement with design values, and the capsule was moved into two successive core positions to achieve design temperatures.

Capsules 61 and 64 completed their scheduled irradiation exposure in June 1963. The thermocouple temperature records of Specimens 61T, 61B, 64T, and 64B contained in these capsules are given in Figs. 22 and 23. The calculated temperatures at the critical portions of the specimen (fuel center, clad ID, and clad OD) are given in Figs. 24 and 25. The average irradiation conditions for each specimen are summarized in Table 21. The specimen temperatures were calculated from the thermocouple readings by using the measured specimen heat generation rates in conjunction with analytically and experimentally determined constants. The method of calibrating the capsule to obtain heat generation rates has been described previously.*

The variations in temperature, even during one reactor cycle, are considerable. The cause of these variations is the shifting flux pattern within the reactor. Temperature fluctuations are particularly severe in high power irradiations, such as these, since relatively small flux changes cause large temperature changes. Methods of temperature control by electrical heaters are not effective because the heaters can only contribute a small fraction of the total fission heat.

---

*J. Cihi, United Nuclear contribution to the AEC Meeting on Problems in Irradiation Capsule Experiments held in Washington, D.C., October 1963. To be published by TID.

Table 20 — Summary of Average Operating Conditions of Specimens 62, 63, 65, and 66 During GETR Cycle 47 (September 1963)

(Temperatures rounded off to nearest 5°)

	Capsule Number and Original Startup Date			
	62 (12/19/62)	63 (1/29/63)	65 (4/6/63)	66 (3/3/63)
Temperature of Fuel Center, °C (°F)				
Upper specimen	1135 (2070)	990 (1810)	1150 (2105)	995 (1825)
Lower specimen	1165 (2125)	925 (1700)	1175 (2150)	1150 (2105)
Temperature of Clad Surface, °C (°F)				
Upper specimen	720 (1330)	470 (880)	430 (805)	460 (865)
Lower specimen	725 (1335)	442 (825)	460 (860)	515 (960)
Specimen Heat Generation Rate, w/cm (kw/ft)				
Upper specimen	371 (11.3)	444 (13.5)	569 (17.3)	414 (12.6)
Lower specimen	394 (12.0)	417 (12.7)	565 (17.2)	496 (15.1)
Cumulative Burnup				
Average, fiss/cm^3	10×10^{20}	10.3×10^{20}	8.7×10^{20}	8.2×10^{20}
(MW-d/T)	(30,000)	(30,700)	(26,400)	(24,600)
Target Burnup				
Average, fiss/cm^3	10.4×10^{20}	20.8×10^{20}	10.4×10^{20}	20.8×10^{20}
(MW-d/T)	(34,000)	(68,000)	(34,000)	(68,000)

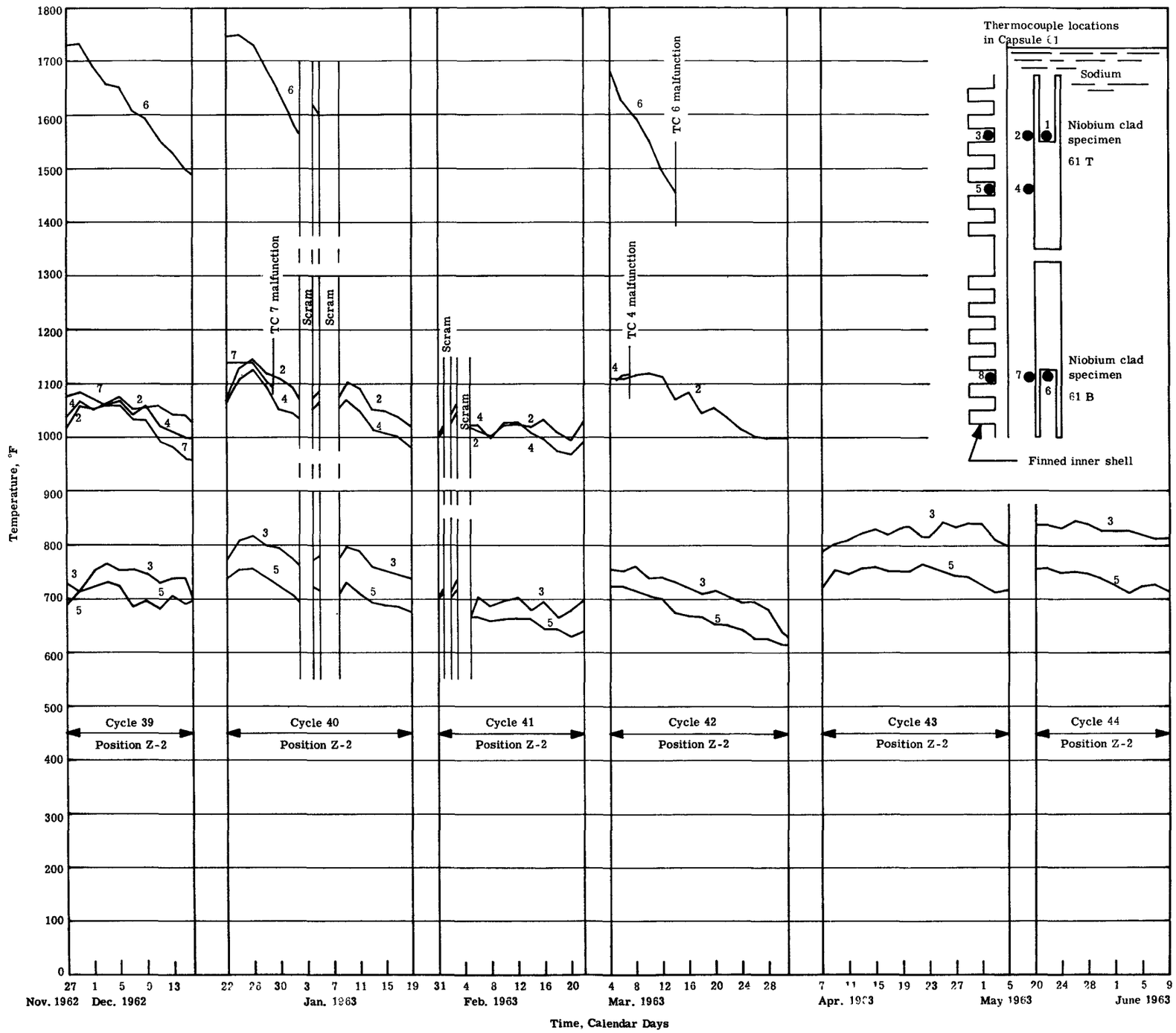

Fig. 22 — Thermocouple records – 61T and 61B

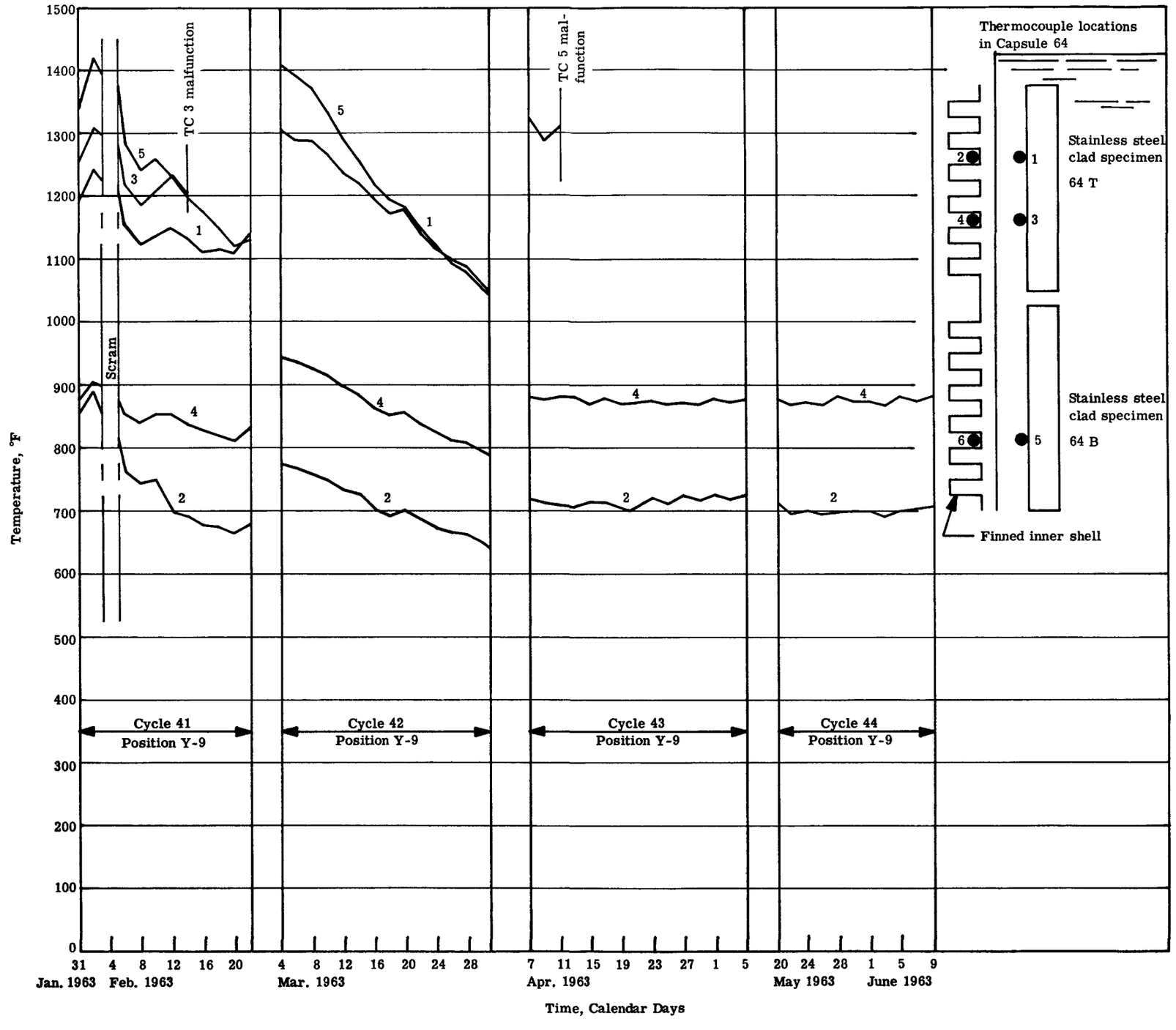

Fig. 23 — Thermocouple records – 64T and 64B

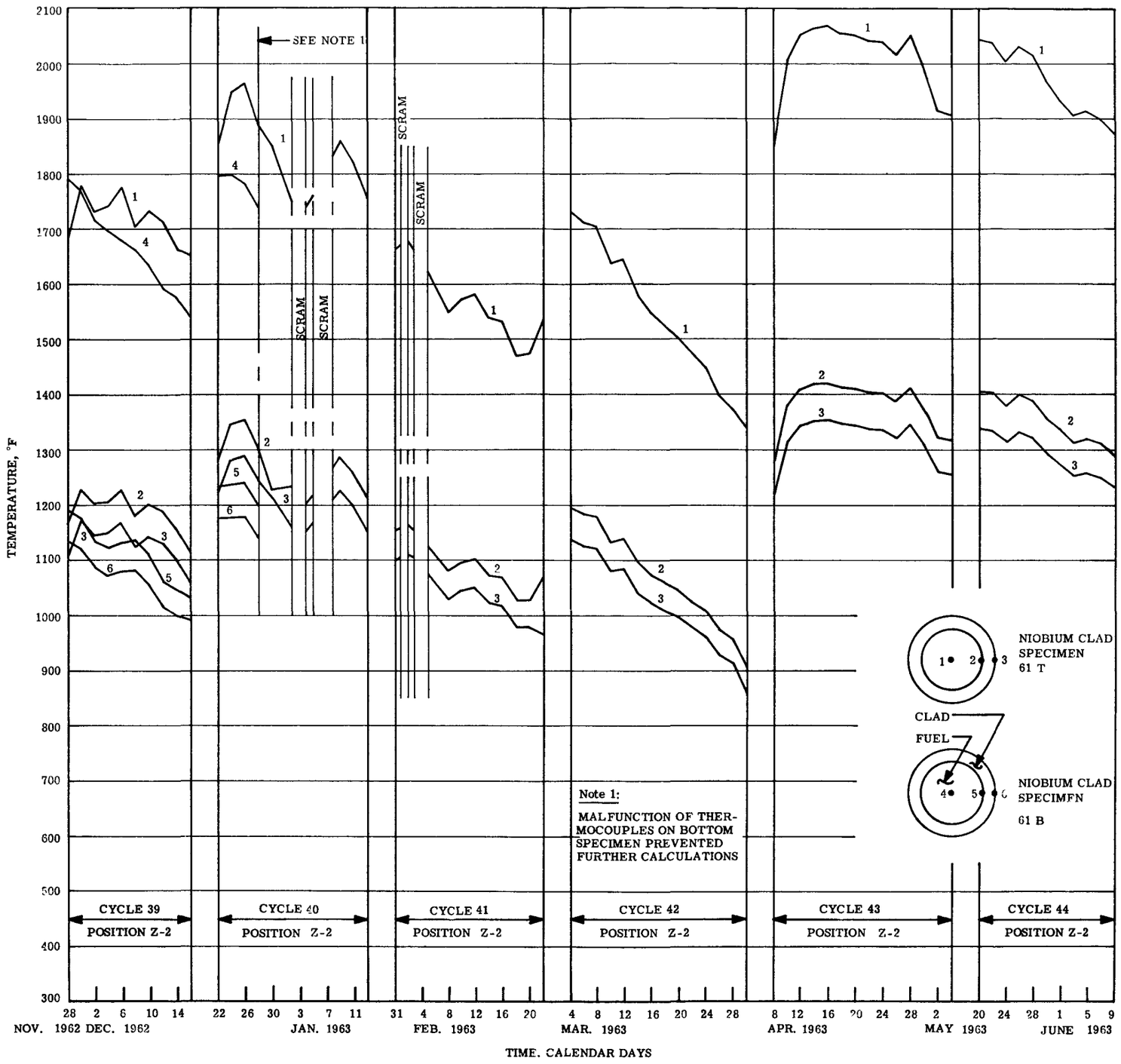

Fig. 24 — Specimen temperature histories – 61T and 61B

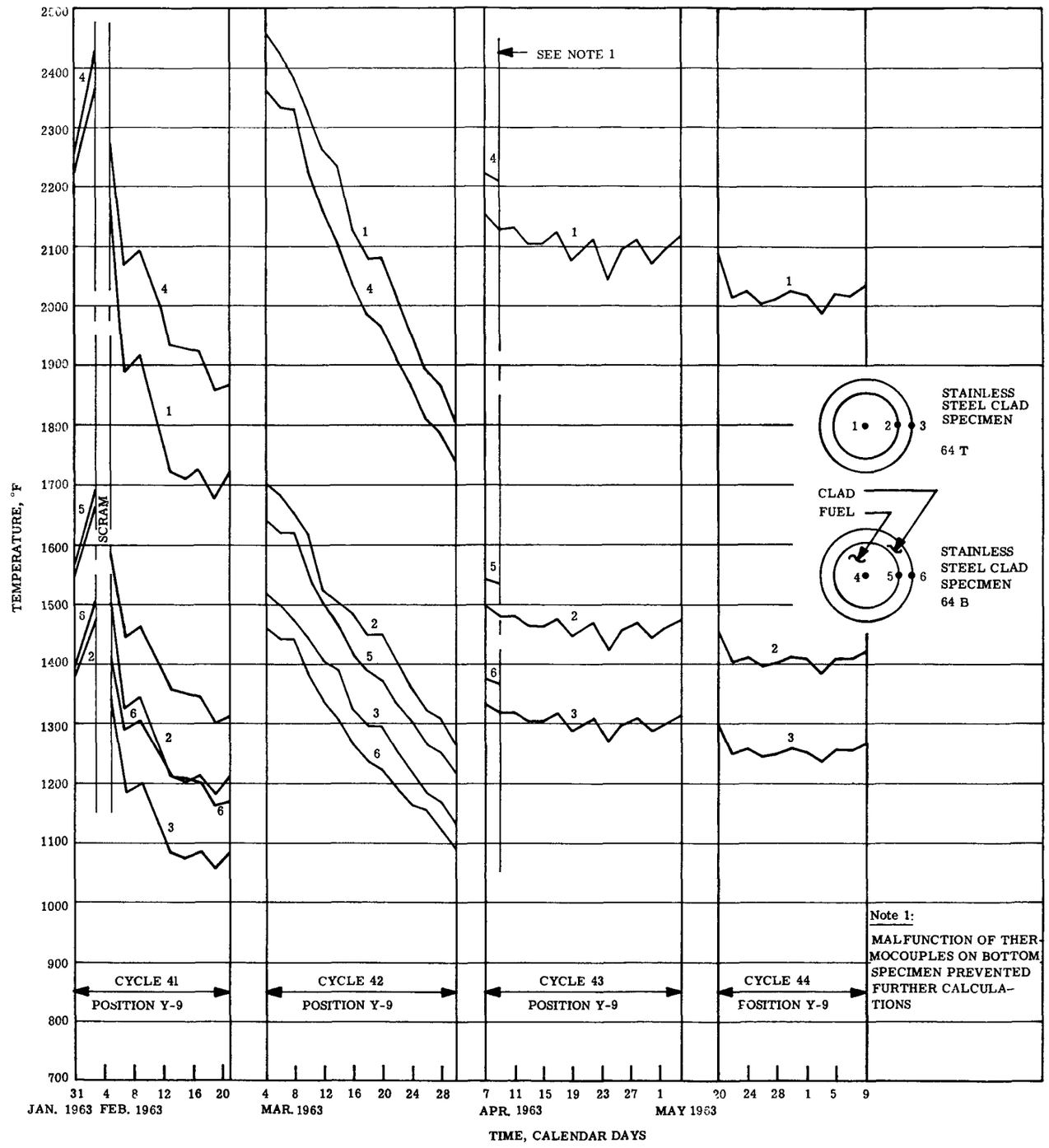

Fig. 25 — Specimen temperature histories – 64T and 64B

Table 21 — Summary of Irradiation Conditions for Specimens 61T, 61B, 64T, and 64B

	Specimen 61T	Specimen 61B	Specimen 64T	Specimen 64B
Fuel Material	$(U_{0.8}Pu_{0.2})C_{0.95}$ +0.1 w/o Ni	$(U_{0.8}Pu_{0.2})C_{0.95}$	$(U_{0.8}Pu_{0.2})C_{0.95}$	$(U_{0.8}Pu_{0.2})C_{0.95}$ +0.1 w/o Ni
Clad Material	Nb	Nb	Type 316	Type 316
Burnup				
fiss/cm^3	6.94×10^{20}	6.83×10^{20}	5.0×10^{20}	5.21×10^{20}
(MW-d/T)	(20,800)	(21,400)	(15,700)	(15,600)
Fuel Center Temperature,* °C (°F)				
Maximum	1305 (2380)	1280 (2340)	1315 (2400)	1415 (2480)
Average	1030 (1890)	1015 (1860)	1125 (2060)	1175 (2150)
Clad ID Temperature,* °C (°F)				
Maximum	840 (1540)	815 (1500)	830 (1530)	900 (1655)
Average	660 (1220)	650 (1200)	735 (1355)	765 (1410)
Clad OD Temperature,* °C (°F)				
Maximum	795 (1460)	770 (1420)	740 (1360)	795 (1460)
Average	625 (1160)	615 (1140)	655 (1215)	690 (1270)
Specimen Heat Generation Rate, w/cm (kw/ft)				
Maximum	450 (13.7)	440 (13.4)	470 (14.4)	510 (15.5)
Average	355 (10.9)	350 (10.7)	380 (11.6)	395 (12.1)
Clad Surface Heat Flux, w/cm^2				
Maximum	210	205	220	240
Average	165	165	180	185
Fuel Power Density, kw/cm^3				
Maximum	2.45	2.40	2.55	2.75
Average	1.95	1.90	2.05	2.15
$\int_{T_s}^{T_c} k\, d\theta$, w/cm				
Maximum	35.8	35.0	37.4	40.6
Average	28.3	27.9	30.3	31.5
Integrated Flux at Specimen Surface, nvt				
Thermal	4.35×10^{20}	4.35×10^{20}	2.84×10^{20}	2.84×10^{20}
0.17 ev to 0.18 Mev	2.46×10^{20}	2.46×10^{20}	1.54×10^{20}	1.54×10^{20}
>0.18 Mev	1.64×10^{20}	1.64×10^{20}	1.02×10^{20}	1.02×10^{20}
Hours of Operation	3267	3267	2189	2189

*Temperatures are rounded off to nearest 5 degrees.

4.3 IN-PILE THERMAL CONDUCTIVITY

An estimate of the in-pile thermal conductivity of $(U_{0.8}Pu_{0.2})C_{0.95}$ and $(U_{0.8}Pu_{0.2})C_{0.95}$ + 0.1% Ni indicated that both materials were in the range of 0.029 to 0.059 cal/sec-cm^2-°C/cm in the temperature range of 700 to 1010°C. The average of three specimens was 0.046 cal/sec-cm^2-°C/cm. The (UPu)C fuel conductivity values are an average of 84% of the UC value of 0.055 cal/sec-cm^2-°C/cm at these temperatures, and are in the range of the Los Alamos out-of-pile measurements of arc cast $(U_{0.8}Pu_{0.2})C$ up to 400°C. Harwell room temperature conductivities of $(U_{0.85}Pu_{0.15})C$ are about 70% of the UC value.

The estimate was obtained by measurement of the temperature drop from fuel center to clad surface, and knowledge of specimen heat generation rate of the clad fuel rods. A typical specimen and irradiation capsule schematic is shown in Fig. 26. The heat generation rate is obtained from the temperature drop between Thermocouple No. 1 and the water temperature. The temperature drop vs heat generation rate calibration is obtained by the input of a known amount of power into the electrical heater and measuring the resulting temperature drop at various reactor power levels.*

The temperature drop from the fuel center to fuel clad surface gives the combined fuel, helium gap, and clad conductivity. The temperature drop across clad can be calculated and subtracted from the total measured temperature drop, since the clad conductivity is known. The resulting fuel center to clad ID temperature drop is used to calculate the combined fuel and gap conductivities. Identical specimens of UC and (UPu)C were irradiated and combined fuel and gap conductivities were measured. From the relatively well known thermal conductivity of UC, a gap conductance of 1.00 w/cm^2-°C was determined. This value was then

---

*J. Cihi, United Nuclear contribution to the AEC Meeting on Problems in Irradiation Capsule Experiments held in Washington, D.C., October 1963. To be published by TID.

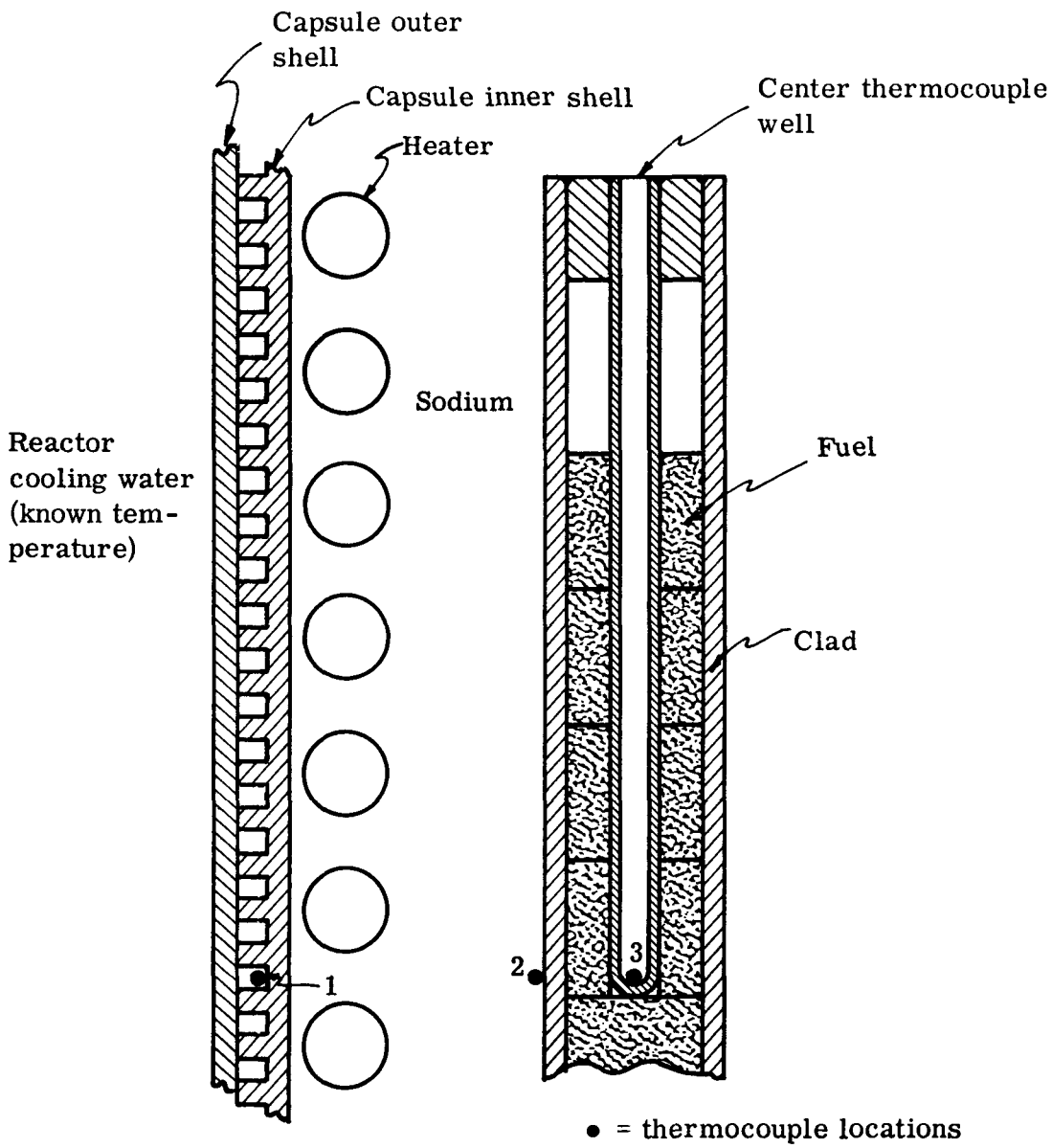

Fig. 26 — Schematic of in-pile thermal conductivity measurement

used to calculate the conductivity of the (UPu)C. The UC gap conductance results were reported previously in Table 4.4 of NDA 2162-5. Improved values, corrected for nonuniform heat generation, are reported here in Table 22.

In irradiations of $(U_{0.8}Pu_{0.2})C$, a 1 w/cm^2/°C gap conductance was assumed at startup, and the fuel conductivities were calculated at that time. Subsequent fluctuations (generally a rise) of the overall fuel plus helium gap conductivity were attributed to changes in conductance rather than the less probable changes in fuel conductivity. The changes in conductance can be caused easily by changes in fuel dimensions. Typical curves of fuel plus helium gap conductivities and calculated gap conductances during a reactor cycle are shown in Fig. 27.

4.4 POST-IRRADIATION EXAMINATION OF CAPSULES 61 AND 64

4.4.1 Summary

The post-irradiation examination was nearly completed for four clad specimens of $(U_{0.8}Pu_{0.2})C_{0.95}$ (Nos. 61T, 61B, 64T, and 64B) irradiated to 5.0 to 6.8 $\times 10^{20}$ fiss/cm^3 (15,700 to 21,400 MW-d/T). The results showed that the stability of the fuel, under the conditions tested, is excellent.

The clad dimensions of the four specimens did not change, with the exception of a localized failure on one specimen. The fission gas release was low, the amount expected from recoil. The fuel dimensional changes were relatively small, up to 5% volume increase, and the microstructure of the fuel was essentially unchanged.

The fuel was compatible with niobium and type 316 stainless steel cladding in helium at the normal operating temperatures and the cladding had good room temperature ductility after irradiation. The cause for a 3/8-in. long fused section on one stainless clad specimen could not be determined definitely. The cause is believed to be an irradiation capsule operating defect.

Table 22 — Helium Gap Conductances (w/cm^2-°C) for UC Irradiation Specimens

Burnup, MW-d/T	Startup	Startup	2500	3800	6500*
Specimen	Type 316†	Nb	Nb	Nb	Nb
UC Thermal Conductivity (assumed), cal/sec-cm-°C					
0.041	1.25	1.08	1.05	1.05	1.21
0.050	1.11	0.97	0.97	0.94	1.16
0.058	1.02	0.91	0.91	0.88	1.08

*Central thermocouple in niobium clad specimen failed shortly after specimen achieved 6500 MW-d/T preventing further calculations of gap conductance for this specimen.

†Central thermocouple in stainless steel clad specimen failed shortly after startup preventing further calculations of gap conductance for this specimen.

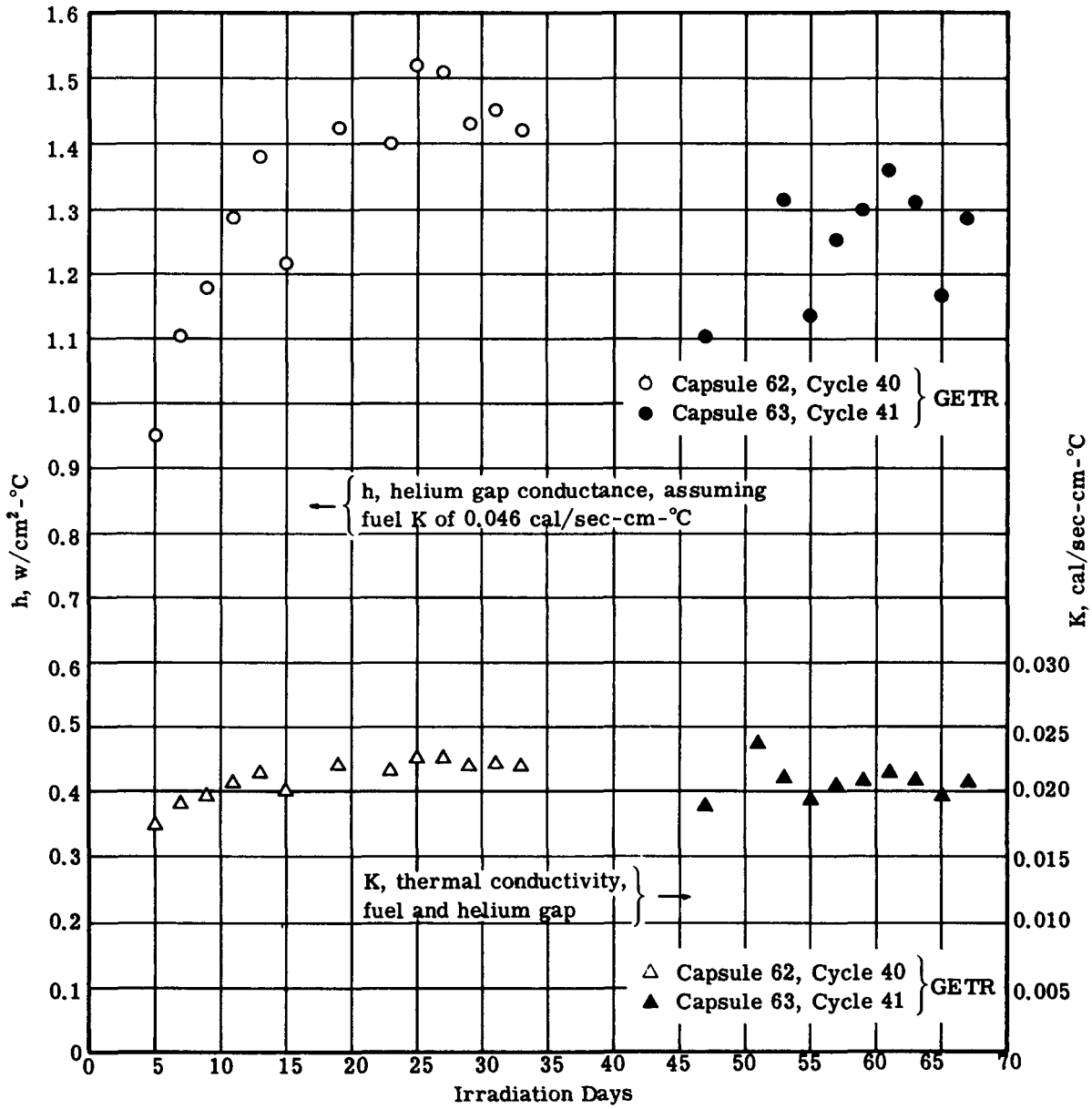

Fig. 27 — Typical in-pile measurements of conductivities and conductances. A gap conductance (h) of 1 w/cm²-°C assumed at startup; k_{fuel} calculated as 0.046 cal/sec-cm-°C at startup from h and measured $k_{fuel + He\ gap}$ (lower curves). Post-startup h (upper curves) calculated assuming k_{fuel} constant.

The post-irradiation examination results to date are summarized in Table 23.

The examination is being made at Battelle Memorial Institute.

4.4.2 Visual Examination and Gamma Scanning

The post-irradiation examination of Capsules 61 and 64 was initiated in July 1963 at Battelle Memorial Institute.

The clad specimens, Nos. 61T, 61B, and 64T were in excellent condition and their diameters were unchanged by the test. Specimen 64B was sound, except for a 3/8-in. center section which had melted and ruptured. An indication of the rupture was given by fission gases found during gas sampling the Capsule 64 inner shell. The failure was highly localized, and the remainder of the specimen was not affected. The diameter changes, even near the failed section, were negligible. The cause of failure has not been determined, but is believed to be a sodium bonding defect in the irradiation capsule, rather than any intrinsic property of fuel or clad. The four specimens are shown in Fig. 28.

The irradiation capsules and specimens were both gamma scanned by counting gamma activity emanating from Zr^{95}-Nb^{95}. The results showed that no fuel was spilled from the specimens, nor was there any detectable fuel movement within the specimens.

4.4.3 Fission Gas Release

The fission gas release from Specimens 61T, 61B, and 64T was low and about what would be expected from recoil. The 13% gas release from failed Specimen 64B is based on the gas analysis of the inner shell of Capsule 64B, and it corresponds to complete release of gas from the two pellets involved in the failed section.

The results are summarized in Table 23.

Table 23 — Summary of Post-Irradiation Examination Results

Specimen	Capsule 61 Top	Capsule 61 Bottom	Capsule 64 Top	Capsule 64 Bottom
Fuel	$(U_{0.8}Pu_{0.2})C_{0.95}$ +0.1 w/o Ni	$(U_{0.8}Pu_{0.2})C_{0.95}$	$(U_{0.8}Pu_{0.2})C_{0.95}$	$(U_{0.8}Pu_{0.2})C_{0.95}$ +0.1 w/o Ni
As fabricated density, % of theoretical	96.0	92.0	92.0	96.0
Clad	Nb	Nb	Type 316	Type 316
Burnup				
fiss/cm^3	6.9×10^{20}	6.8×10^{20}	5.0×10^{20}	5.2×10^{20}
(MW-d/T)	(20,800)	(21,400)	(15,700)	(15,600)
Clad OD changes	Negligible	Negligible	Negligible	Negligible, except for 3/8-in. long molten section
Fission gas release, % of total				
Gamma Spec. 1	0.10	0.11	0.22	13.15
Gamma Spec. 2	0.13	—	0.24	12.58
Mass Spec.	0.37	0.25	0.75	—
Number of pellets				
Whole	4	9	—	7
Cracked	12	7	Shattered with light handling	4 – in failed section
Fuel OD changes, avg % (+)	1.5	1.4	—	1.6
Volume changes, avg % (–)	1.7	4.1	—	5.1
Density changes by weight and volume, avg % (–)	2.5	4.3	—	3.8
Porosity by point counting				
Pre-irradiation	1.0	7.6	7.6	1.0
Post-irradiation	5.3 to 9.4	8.7 to 13.7	9.0 to 13.5	3.5 to 4.2 (adjacent to failure)
Fuel metallography	As before	As before without dicarbide	As before without dicarbide	As before, except in failed section
Clad metallography	No fuel-clad reaction	No fuel-clad reaction	No fuel-clad reaction	Reaction in failed section and opposite pellet interfaces
Clad bend tests	Ductile	Ductile	Ductile	Less ductile than 64T

SPECIMEN NUMBER

61T 61B 64T 64B

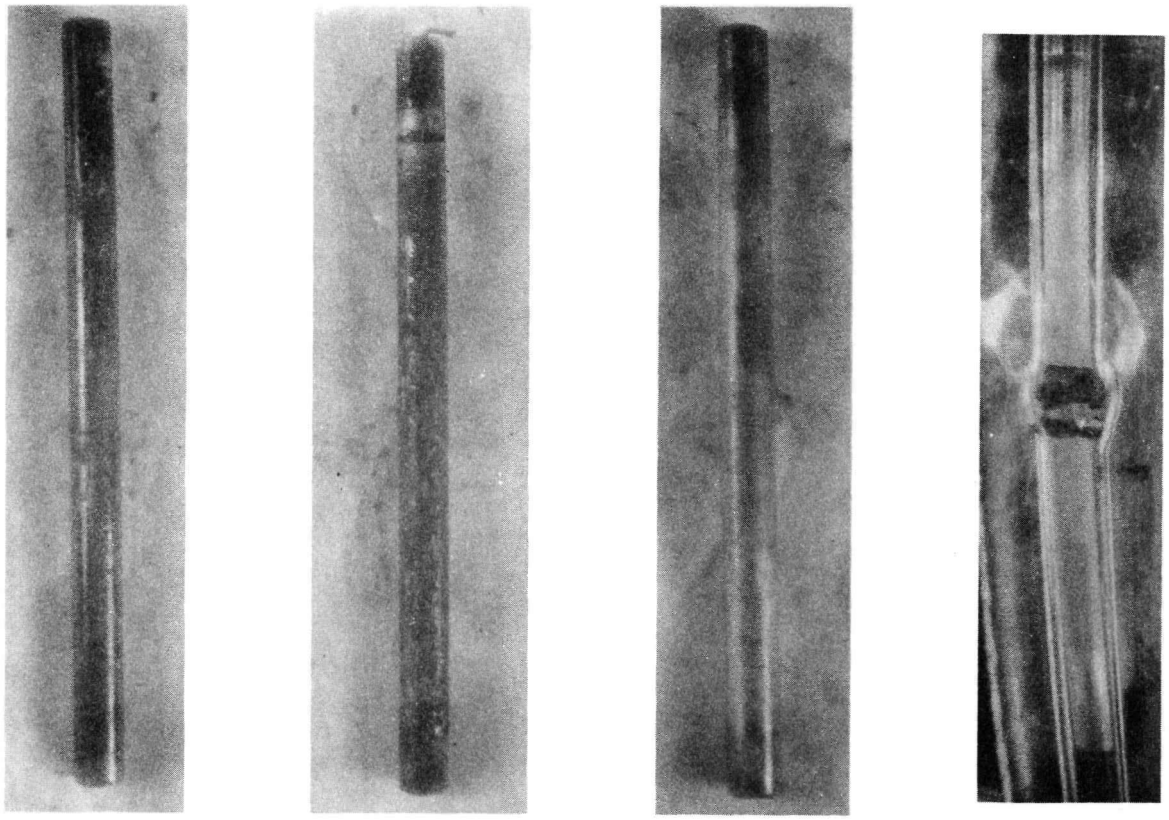

Fig. 28 — Clad $(U_{0.8}Pu_{0.2})C_{0.95}$ fuel specimens after irradiation

The gas samples were taken by puncturing the capsule inner shell, and subsequently the sample cladding, in a completely sealed, leaktight, evacuated system. The gas released from the capsule was transferred by a Toepler pump to a system of known volume. The total quantity of gas was calculated from the system volume and gas pressure.

Known volume sample vials containing the gas were sealed off and analyzed by gamma and mass spectrography.

4.4.4 Macro Examination

Fuel

The cladding was slit longitudinally to remove the fuel. Care was taken not to touch the fuel with the cutting wheel. The fuel was extremely brittle after irradiation; and the clad cutting operation and subsequent handling contributed to fuel cracking. Decladding was successful in leaving about one-third of the fuel pellets intact. Most of the remainder were cracked in large pieces (Fig. 29). The surface appearance of the fuel was the same as before irradiation. There was no significant difference between the appearance of fuel made with and without sintering aid.

Dimensional changes measured on whole pellets were isotropic: 0.002 to 0.003-in. increase on an original 0.191 in. OD, and on a variable original length of 0.185 to 0.192 in. Volume and density changes calculated from weights and volumes agreed fairly well and were in the range of 2 to 5%. Again, sintering aid made no difference. The results of all measurements are given in Table 24, the averages are given in Table 23.

Immersion densities in carbon tetrachloride gave widely scattered results and are not believed to be as reliable.

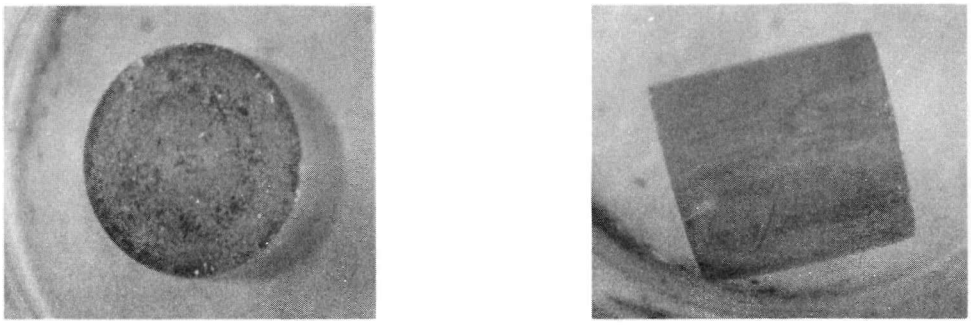

Typical whole pellet – $(U_{0.8}Pu_{0.2})C_{0.95}$ + 0.1 w/o Ni irradiated to 6.9×10^{20} fiss/cm^3 (from specimen 61T) 6×

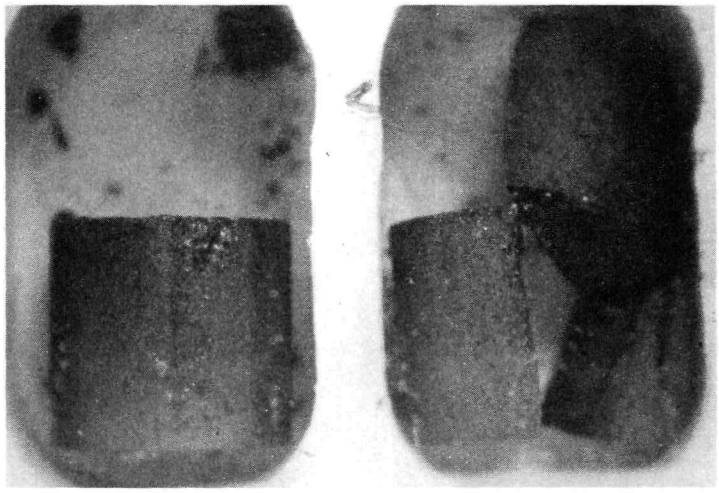

Typical whole and cracked pellet – $(U_{0.8}Pu_{0.2})C_{0.95}$ irradiated to 6.8×10^{20} fiss/cm^3 (from specimen 61B) 6×

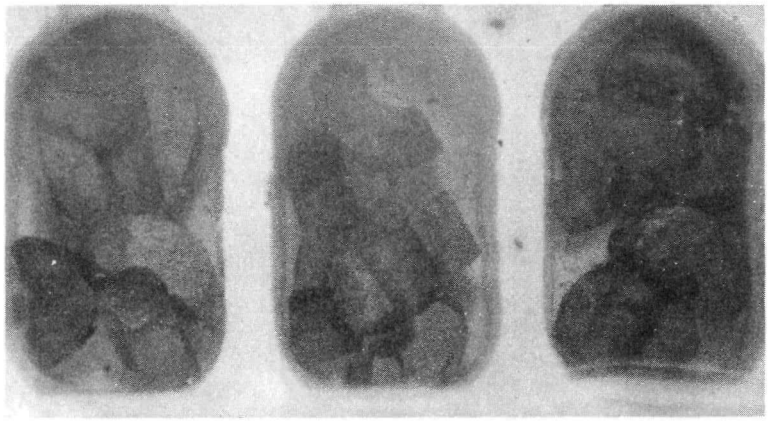

Typical cracked pellets – $(U_{0.8}Pu_{0.2})C_{0.95}$ + 0.1 w/o Ni irradiated to 6.9×10^{20} fiss/cm^3 (from specimen 61T) 4×

Fig. 29 — Typical irradiated fuel pellets

Table 24 — Dimensional and Density Measurements of Whole Pellets

Pellet No.	Pellet Diameter, in. Pre-Irradiation	Pellet Diameter, in. Post-Irradiation	Diameter Change, %	Pellet Length, in. Pre-Irradiation	Pellet Length, in. Post-Irradiation	Length Change, %	Pellet Volume, cm^3 Pre-Irradiation	Pellet Volume, cm^3 Post-Irradiation	Volume Change, %	Pellet Weight, g Pre-Irradiation	Pellet Weight, g Post-Irradiation	Pellet Density, g/cm^3 Pre-Irradiation	Pellet Density, g/cm^3 Post-Irradiation*	Pellet Density, g/cm^3 Post-Irradiation†	Density Change, % By Weight and Volume	Density Change, % By Immersion
61T-6	0.1902	0.1937	1.84	0.1886	0.1887	0.05	0.0879	0.0912	3.75	1.175	1.1415	13.23	12.52	12.568	-5.44	-5.00
-8	0.1907	0.1932	1.31	0.1915	0.1985	3.65	0.0897	0.0906	1.00	1.195	1.2062	13.20	13.31	12.621	+0.83	-4.39
-9	0.1910	0.1934	1.26	0.1944	0.1905	-2.01	0.0914	0.0918	0.44	1.175	1.1551	12.86	12.59	—	-2.10	—
61B-3	0.1910	0.1936	1.36	0.1953	0.1979	1.33	0.0918	0.0955	4.03	1.144	1.1373	12.46	11.90	—	-4.50	—
-4	0.1904	0.1930	1.36	0.1936	0.1961	1.29	0.0904	0.0942	4.20	1.127	1.1398	12.47	12.10	—	-2.97	—
-5	0.1900	0.1928	1.47	0.1912	0.1934	1.15	0.0890	0.0926	4.05	1.098	1.1117	12.34	12.01	11.920	-2.68	-3.40
-7	0.1907	0.1932	1.31	0.1910	0.1930	1.05	0.0896	0.0928	3.57	1.115	1.0388	12.44	11.20	—	-9.96	—
-8	0.1899	0.1922	1.21	0.1885	0.1911	1.38	0.0876	0.0910	3.88	1.080	1.0949	12.35	12.03	11.867	-2.40	-3.91
-9	0.1899	0.1930	1.63	0.1900	0.1920	1.05	0.0882	0.0922	4.54	1.092	1.1067	12.40	12.00	—	-3.22	—
64T-6	0.1908	—	—	0.1920	0.1950	1.56	0.0900	—	—	1.120	—	12.45	—		—	
64B-2	0.1912	—	—	0.1940	—	—	0.0914	—	—	1.160	1.1609	12.70	—	11.467	—	
-11	0.1907	0.1938	1.62	0.1923	0.1955	1.66	0.0901	0.0946	5.00	1.163	1.1760	13.00	12.44	12.611	-4.31	-2.99
-12	0.1904	0.1940	1.89	0.1924	0.1953	1.51	0.0898	0.0947	5.46	1.159	1.1881	12.90	12.55	—	-2.71	—
-13	0.1913	0.1942	1.52	0.1929	0.1956	1.40	0.0910	0.0951	4.51	1.174	1.1910	12.90	12.53	—	-2.87	—
-14	0.1914	0.1941	1.41	0.1940	0.1987	2.42	0.0916	0.0965	5.35	1.173	1.1771	12.81	12.14	—	-5.23	—

*Density determined by weights and dimensions.
†Density measured by immersion techniques.

Clad

Strips from the niobium clad specimens (Nos. 61T, 61B) and the sound type 316 clad specimen (No. 64T) were very ductile and could be bent 180° over a 1/2 in. radius without cracking. The type 316 clad from the ruptured specimen (No. 64B) was less ductile and broke before 110°.

The ID of all the clads appeared to be in good condition by macro examination. The location of pellet interfaces could be identified by different shadings. Fig. 30 shows the ID of the bent cladding samples.

4.4.5 Micro Examination

Fuel

Significant changes in fuel microstructure did not occur. The $(U_{0.8}Pu_{0.2})C_{0.95}$ + 0.1 w/o Ni retained its monocarbide-sesquicarbide structure (Fig. 31). The $(U_{0.8}Pu_{0.2})C_{0.95}$ was single-phase monocarbide after irradiation, having lost any trace of original dicarbide (Fig. 32).

The grain size or shape was not changed by irradiation, and there was no change in grain size radially within any specimen. The porosity increased uniformly in about the proportion of the volume increase, as measured by point counting.

The observations apply to all specimens including the sound portions of 64B. The examination of the ruptured portion of 64B is described subsequently.

Clad, Type 316

No interactions occurred between the fuel and the type 316 cladding in Specimen 64T. Several radial and longitudinal sections were examined. Typical pre- and post-irradiation structures are compared in Fig. 33.

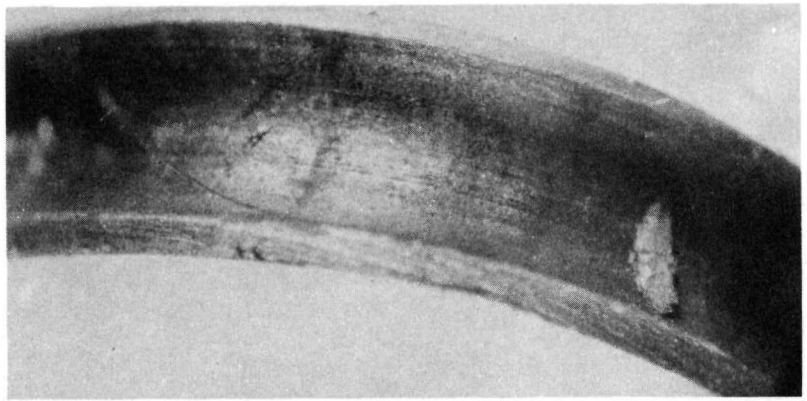

Specimen 61T – 6×

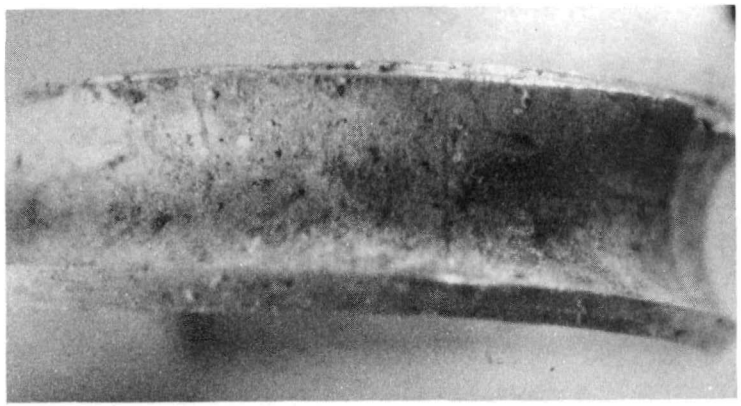

Specimen 64T – 6×

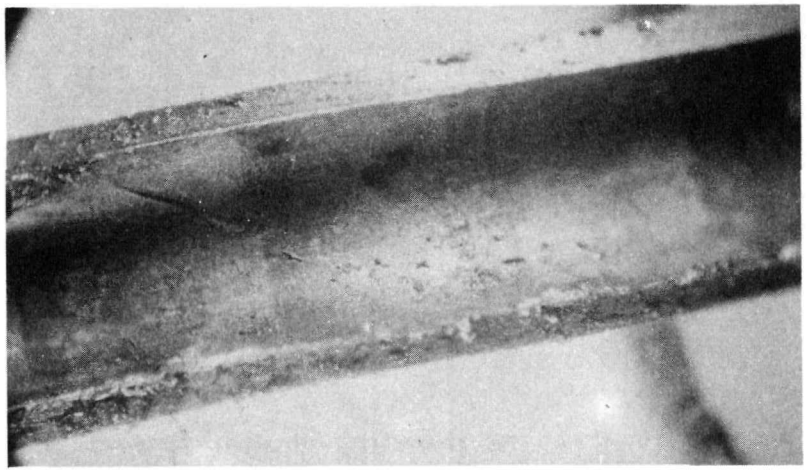

Specimen 61B – 6×

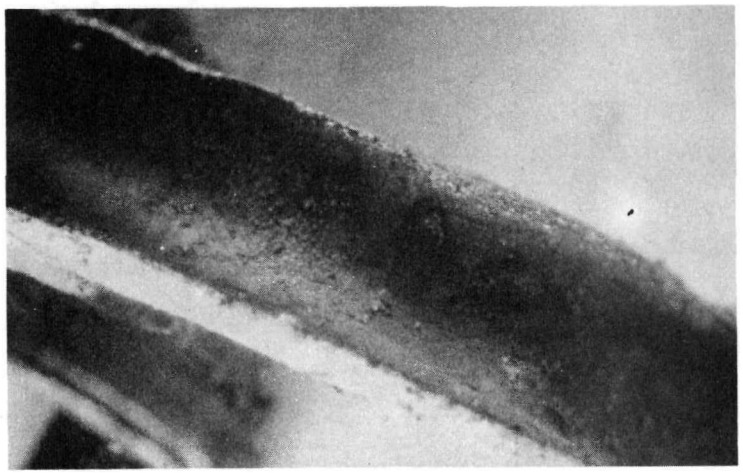

Specimen 64B – 6×

Fig. 30 — ID of clad bend tests

Pre-irradiation – 600×

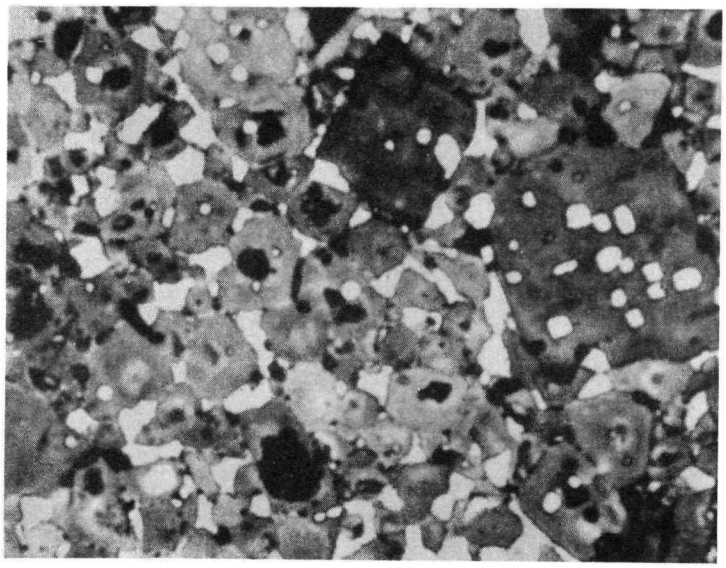

Post-irradiation (5.2×10^{20} fiss/cm^3) – Specimen 64B – 600×

Fig. 31 — $(U_{0.8}Pu_{0.2})C_{0.95}$ + 0.1 w/o Ni microstructure

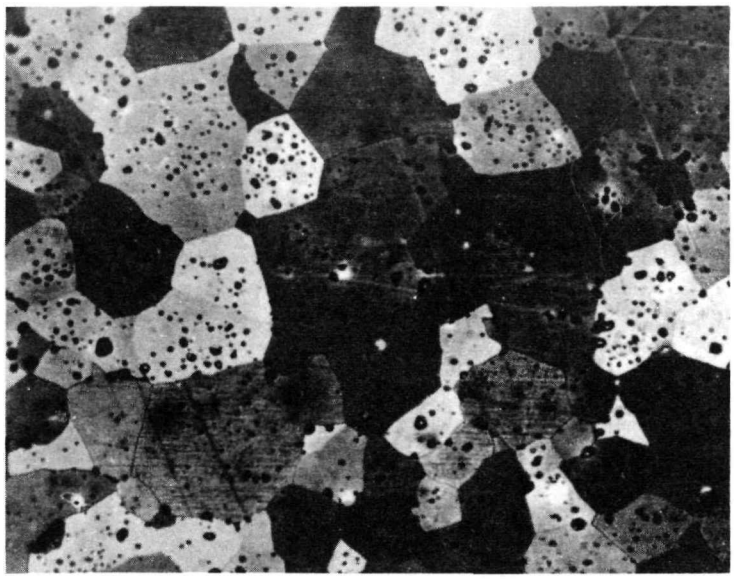

Pre-irradiation – 250×

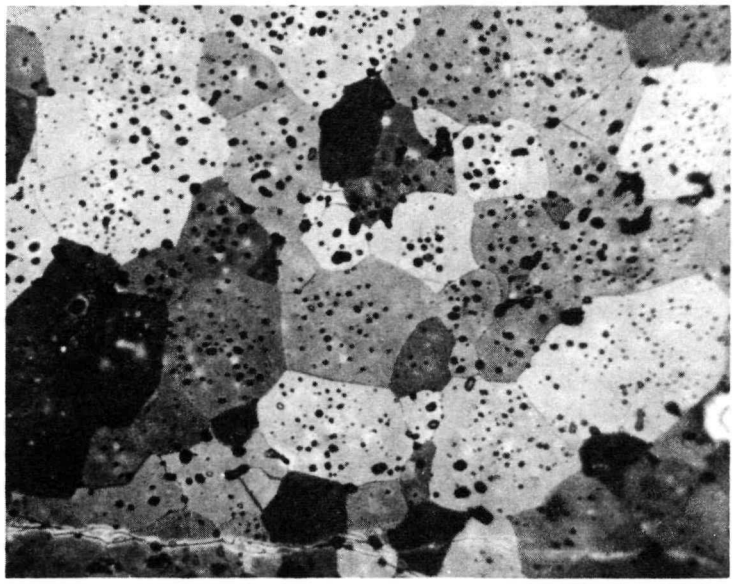

Post-irradiation (6.8×10^{20} fiss/cm^3) – Specimen 61B – 250×

Fig. 32 — $(U_{0.8}Pu_{0.2})C_{0.95}$ microstructure

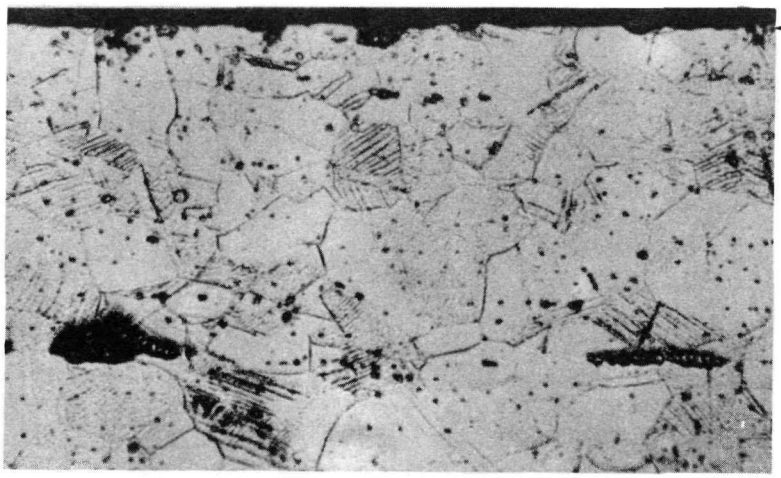

Before irradiation – 250×

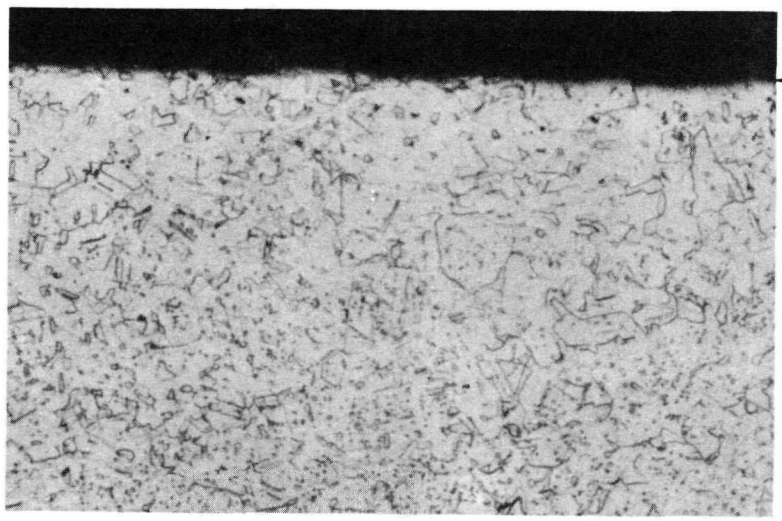

After irradiation for 2190 hr at 730°C avg
and 840°C max. clad ID – Specimen 64T – 250×

Fig. 33 — Typical type 316 stainless steel clad microstructure after 2190 hr

The structure of the steel changed from the essentially single-phase, austenitic, cold drawn (half-hard) microstructure, to a range of structures produced by the thermal gradient across the clad (austenite containing sigma and carbide precipitate). The presence of carbide was due to carbon precipitation from the steel by a thermal effect rather than carbon diffusion from the fuel. This was shown by the similar structures of the clad adjacent to the fuel and clad from the gas expansion space away from the fuel.

The microhardness of the steel cladding did not change significantly.

	Knoop Hardness, 100 g Load
Before Irradiation	240 to 250
After 5.4×10^{20} nvt (Specimen 64T)	180 to 226

The detailed results are shown in Table 25.

Support Spacer, Niobium

The niobium spacer which supports the column of pellets in Specimen 64B was bonded to the bottom fuel pellet. Metallographic examination of the interface showed that the bond was mechanical and there were no fuel-niobium interactions across the diameter of the niobium disc. The sides of the disc appeared to be slightly carburized.

Specimen 64B Rupture

As part of the effort to resolve the cause of specimen failure, the metallographic examination of Specimen 64B was more extensive than the examination of the other three specimens.

The 3/8-in. long ruptured section is shown in Fig. 34. Radial and longitudinal sections were examined. Representative microstructures from the failed area are shown in Fig. 35.

Table 25 — Microhardness of Irradiated Type 316 Cladding
(Knoop Hardness)

	Specimen 64T			Specimen 64B (Failed Section)			
	Traverse No. 1	Traverse No. 2	Traverse No. 3	Traverse No. 1	Traverse No. 2	Traverse No. 3	
OD	226	223	172	142	178	(OD) 93.1	146
	218	222	164	149	171	123	130
	193	197	173	134		125	148
	189	173	179	146	155	128	137
	193	177					
	191	177	175	140	165	134	147
	198	180	172	143	142	148	127
	193	193	160			137	127
	180	184	163	156	178	134	147
	180	193				125	153
	203	195	164			174	154
	189	226	163	161	146	130	156
ID	226	180	162	198	142		(ID) 179

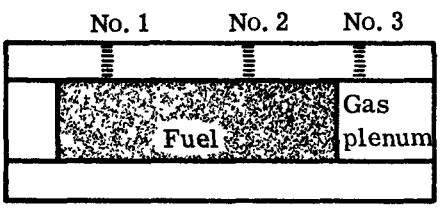

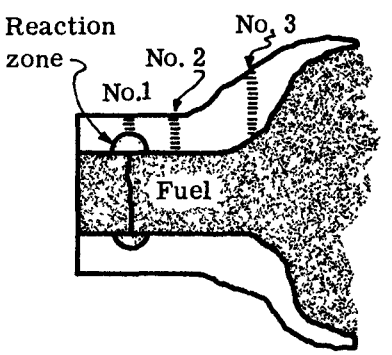

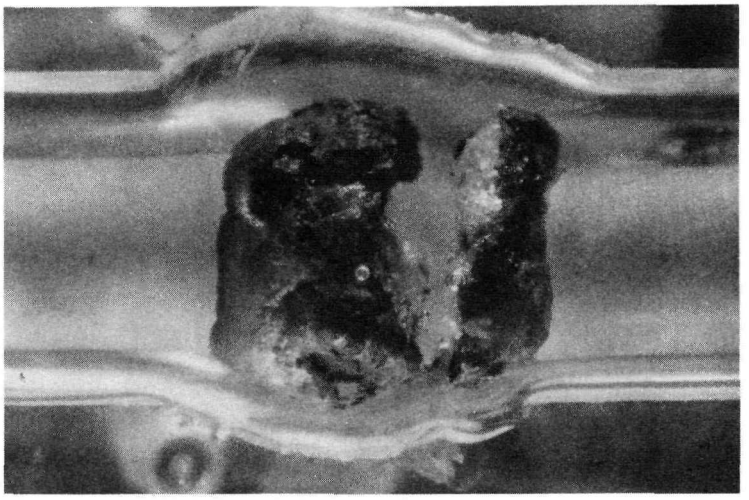

Fig. 34 — Magnification of failed section – Specimen 64B

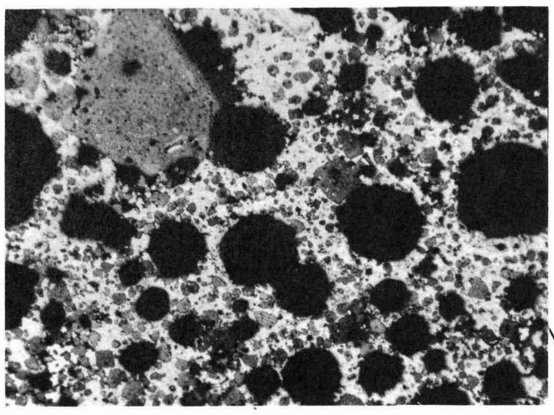

Typical fuel in failed section –250×

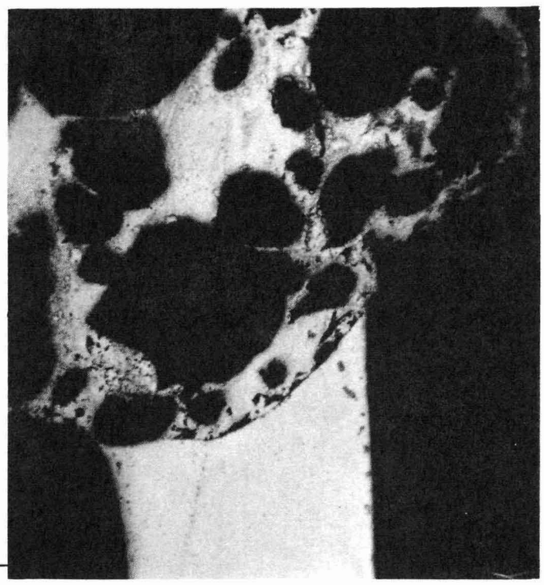

Ruptured clad-fuel interface (no reaction) –100×

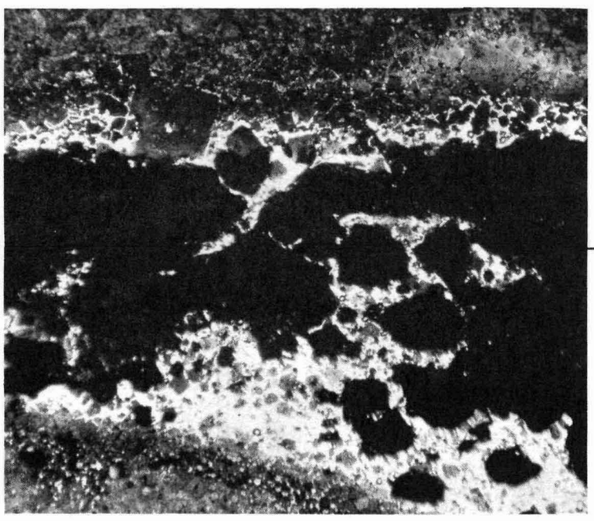

Interface between failed and unfailed fuel sections –100×

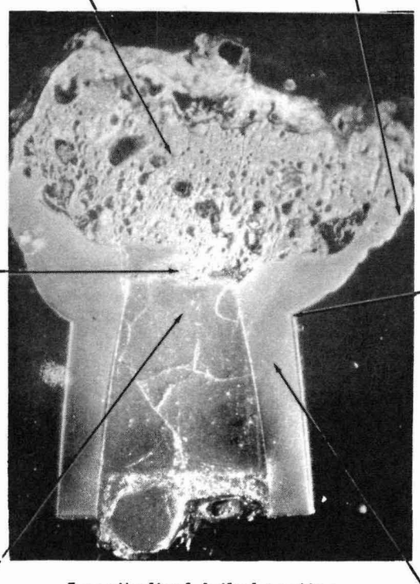

Longitudinal failed section – specimen 64B - 6×

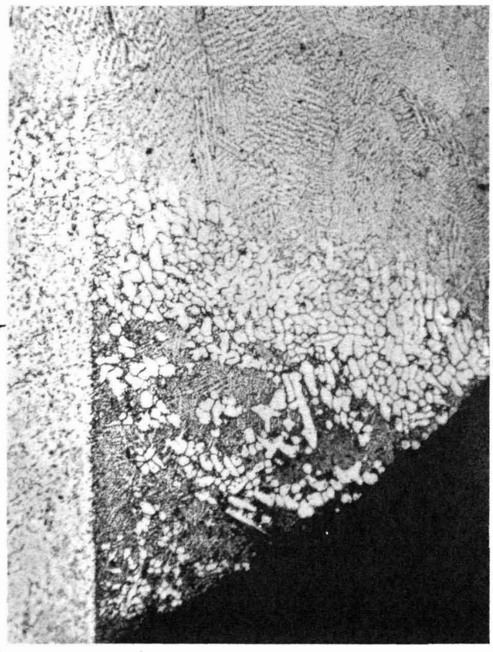

Structures at edge of rupture –100×

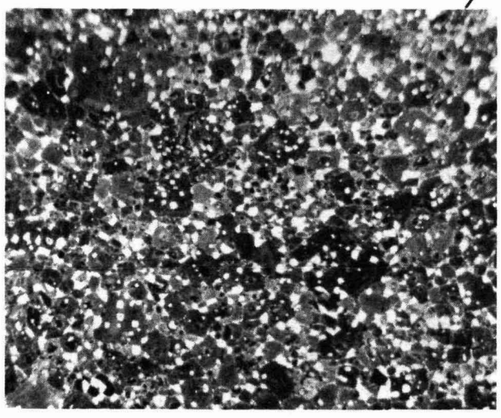

Normal fuel structure adjacent to failure – 250×

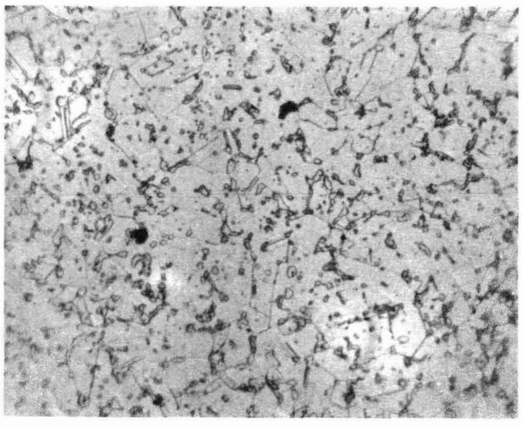

Normal clad structure adjacent to failure –250×

Fig. 35 — Representative microstructures from the failed section

The fuel in the failed area had large bubbles and a spongy appearance showing that very high temperatures had occurred. The relatively small carbide grain size suggests that the temperatures may have been below the melting point of the fuel. In contrast with fuel from the sound part of the specimen, the fuel in the failed section had large connected areas of a light etching phase. A bromine etch known to attack free uranium in carbide fuels did not affect this phase, indicating that the light etching phase is sesquicarbide or dicarbide. The increase in higher carbides would indicate a uranium-plutonium loss from the fuel. Immediately adjacent to the failure, the fuel microstructure was normal.

The clad had as-cast structure at the rupture, indicating that it had been molten. In some areas a fuel-clad interaction had occurred, but in others "molten" fuel had been in contact with steel without a reaction.

At areas immediately adjacent to and away from the failure the clad appeared normal, except for reaction zones opposite pellet interfaces and cracks in the fuel (Fig. 36). The nature of the reaction zone has not been identified. It is etched by a phosphoric acid etchant known to attack iron-plutonium alloys, and a nitric-acetic acid etch known to attack uranium-plutonium carbides. These etchants do not attack the normal stainless steel structure. Microhardness readings, summarized in Table 25, indicate that the reacted zone has about the same hardness as the base metal, and that the zone is not a carburized one. The reaction zone is probably an iron-nickel-uranium-plutonium alloy. Since the reaction zone only appeared opposite cracks in the fuel, and not where the fuel was in good contact with the clad, the transfer of the reacting product (presumably uranium-plutonium) must have been by gas or liquid metal. The sound Specimen 64T did not have such reaction zones and one would conclude that the transfer agent in Specimen 64B was sodium which entered through the rupture.

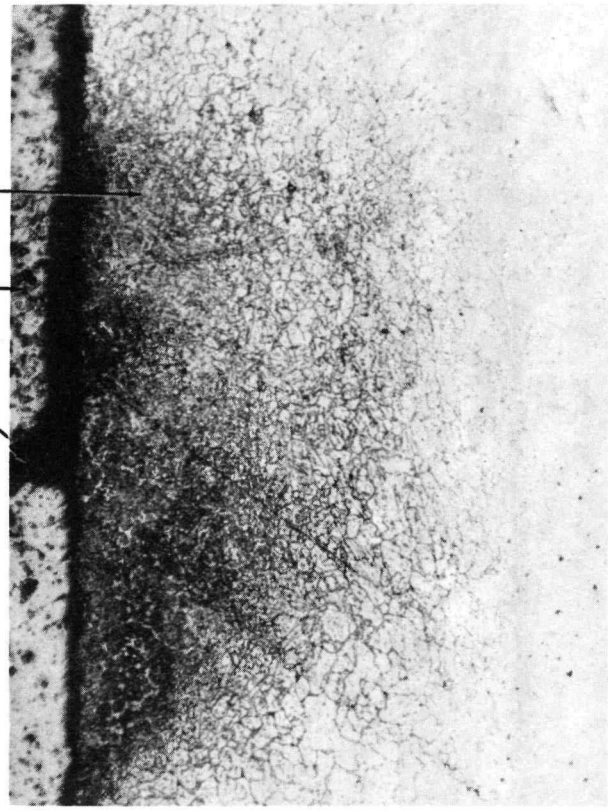

Nitric-acetic-water etch 100×

Fig. 36 — Reaction zones in ruptured type 316 cladding

4.4.6 Plutonium Distribution

Samples for plutonium distribution analysis were obtained by drilling out concentric radial samples from a fuel pellet using diamond drills. Drilling began at the pellet center starting with the smallest size drill (0.080 in.) and progressing through drill sizes of 1/8 in., 5/32 in., and 3/16 in. in that order (a total of four samples from each pellet). The resultant powder samples were thoroughly removed between each drilling. A longitudinal cross section of the pellet after drilling sampling is shown in Fig. 37. Samples were obtained from fuel pellets from Specimens 61T, 61B, and 64B. No pellet from Specimen 64T was sound enough for meaningful sampling.

The samples have been submitted for mass spectrographic analysis to determine uranium-plutonium ratio.

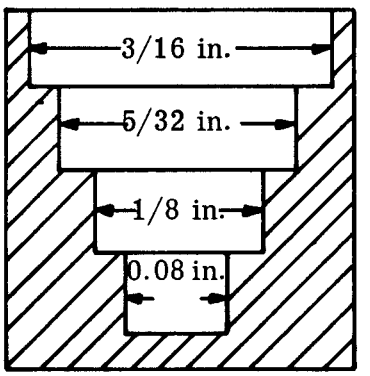

Fig. 37 — Cross section of fuel pellet after removing samples for plutonium distribution analysis

4.4.7 Burnup Determination

Three methods of average burnup determinations are being used:

1. Total heat generation
2. Ni-Co dosimeter wire
3. Mass spectrography for U and Pu isotopes.

Total heat generation is measured by in-pile calorimetry as described in Section 4.2. Knowledge of the fission heat generation and total energy per fission permits calculations of the burnup. All of the burnup figures reported to date are based on this method.

Radiochemical analysis of a Ni-Co dosimeter wire, which had been placed along the length of the specimen, gives good relative burnup figures along the length of the specimen. The wires are being analyzed.

One pellet per specimen was taken for mass spectrographic burnup determination. The relative analyses from the monitor wire in combination with one absolute analysis can be used to obtain absolute burnup numbers along the length of the specimen. The mass spectrograph values are not yet available.

Self-shielding of the central portion of highly enriched fuel in a thermal neutron flux can be considerable. All of the specimens described were irradiated in a thermal neutron flux. It is of importance, therefore, to examine the radial burnup distribution within the fuel. Table 26 is a summary of burnup at the fuel center and fuel OD of each specimen. The burnup distribution was obtained by the use of the STAR code, a one-dimensional, multigroup, diffusion theory code, and the average, heat-generation based, burnup of each specimen.

4.4.8 Hot Cell Handling Procedure

The relatively large plutonium content of the fuel specimens contributed an added hazard to the handling procedures. Normally, of course, plutonium-containing

Table 26 — Radial Variation of Burnup in Fuel

Specimen	Burnup, 10^{20} fiss/cm^3 (MW-d/T) Code Calculated Maximum at Fuel OD	Code Calculated Minimum at Fuel Center	Average Calculated from In-Pile Heat Generation
61T	11.7 (35,400)	2.9 (8,700)	6.9 (20,800)
61B	11.6 (36,400)	2.9 (9,000)	6.8 (21,400)
64T	8.4 (26,700)	2.1 (6,600)	5.0 (15,700)
64B	8.8 (26,500)	2.2 (6,600)	5.2 (15,600)

materials are handled in leaktight glove boxes to prevent the spread of alpha contamination. Also, an inert atmosphere is often employed in these boxes to prevent oxidation or burnup of the more reactive plutonium materials such as PuC. Fortunately, experience at other hot cell facilities indicated that irradiated plutonium could be handled in conventional hot cells as long as the ratio of beta-gamma to alpha activity was greater than 500 to 1. The philosophy behind this handling is that if the more readily detectable beta-gamma activity is detected and removed, the associated alpha activity is also detected and removed. The 500 to 1 ratio means that examination of the fuel material must be conducted within a certain minimum time after removal from the reactor. Calculations indicated that examination of fuel from the lowest burnup samples would have to be completed within about 5 months after reactor shutdown.

As precaution against oxidation and fire, operations involving exposure of fuel were conducted under a plastic canopy which was continuously flushed with dry nitrogen from a liquid nitrogen source. The canopy also provided a means of minimizing the spread of alpha contamination resulting from cutting or grinding operations. To further minimize oxidation, bare fuel was stored under dehydrated

mineral oil. The mineral oil was also used to protect the fuel during viewing and macrophotography operations at the stereo camera.

The mineral oil was not entirely acceptable as an oxidation preventative. Consequently, the use of a vacuum dessicator was started. Likewise, the nitrogen-flushed canopy did not provide an atmosphere completely acceptable for preventing oxidation. However, the atmosphere was acceptable from the standpoint of fire protection, since no fires were experienced and no sparking of fuel was observed in cutting or grinding operations.

Metallography was done in an air cell. The material had sufficient oxidation resistance to permit polishing, etching, and viewing during relatively short periods of air exposure.

DISTRIBUTION

United States Atomic Energy Commission
Division of Reactor Development,
Washington, D. C.
Attn: Mr. J. Simmons,
Chief, Fuels and Materials Development Branch . . . 2

Dr. G. W. Wensch,
Chief, Liquid Metal Cooled Reactors Branch 3

Mr. William Rice 2

New York Operations Office,
New York 14, New York
Attn: Mr. M. Plisner,
Contracts Division (Industrial) 2

Chicago Operations Office,
Argonne, Illinois
Attn: Mr. C. A. Pursel,
Director, Reactor Engineering Division 1

Oak Ridge Operations,
Oak Ridge, Tennessee
Attn: Mr. D. F. Cope,
Director, Reactor Division 1

Hanford Operations Office,
Richland, Washington
Attn: Mr. J. Musser 1

Office of Technical Information
Oak Ridge, Tennessee 3

Brookhaven National Laboratory,
Upton, Long Island, New York
Attn: Mr. H. S. Potter,
Chief, New York Patent Group 1

Oak Ridge National Laboratory,
Oak Ridge, Tennessee
Attn: Mr. J. Frye,
Metallurgy Division 1

Nuclear Materials and Equipment Corporation
Appollo, Pennsylvania
Attn: Mr. K. Puechl, Acting Director,
Advanced Materials Center 1

Argonne National Laboratory,
Lemont, Illinois
Attn: Dr. Frank G. Foote 4

Battelle Memorial Institute,
Columbus, Ohio
Attn: Dr. Russell W. Dayton 1

General Electric Co.,
San Jose, California
Attn: Dr. Karl Cohen 1

Hanford Laboratories Operation, General Electric Co.,
Richland, Washington
Attn: Mr. F. W. Albaugh 1

Monsanto Research Corporation, Mound Laboratory,
Miamisburg, Ohio
Attn: Dr. L. V. Jones 1

Atomics International,
Canoga Park, California
Attn: Dr. Harry Pearlman 1

Dow Chemical Company, Rocky Flats,
Boulder, Colorado
Attn: Mr. J. Willging 1

Los Alamos Scientific Laboratory,
Los Alamos, New Mexico
Attn: Dr. R. Baker 2

Lawrence Radiation Laboratory, University of California,
Berkeley, California
Attn: Dr. Carl Cline (Livermore Lab.) 1

Power Reactor Development Co.,
Detroit, Michigan
Attn: Mr. R. W. Hartwell, General Manager 1